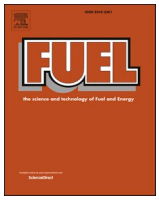
Fuel 357 (2024) 129712



Contents lists available at ScienceDirect

Fuel

journal homepage: www.elsevier.com/locate/fuel



Full Length Article

Solubility and interfacial tension models for CO_2–brine systems under CO_2 geological storage conditions

Meiheriayi Mutailipu [a,b], Yongchen Song [c], Qiang Yao [a,b], Yu Liu [c], J.P. Martin Trusler [d,*]

[a] Engineering Research Center of Northwest Energy Carbon Neutrality, Ministry of Education, Xinjiang University, Urumqi 830017, China
[b] School of Electrical Engineering, Xinjiang University, Urumqi 830017, China
[c] Key Laboratory of Ocean Energy Utilization and Energy Conservation of the Ministry of Education, Dalian University of Technology, Dalian 116024, China
[d] Department of Chemical Engineering, Imperial College London, South Kensington Campus, London SW7 2AZ, United Kingdom

ARTICLE INFO

Keywords:
Carbon geological storage
Solubility
Interfacial Tension
Equation of State
Activity–coefficient model
Phase equilibrium

ABSTRACT

Thermodynamic properties of the CO_2–brine pseudo-binary system are essential for the design of geological carbon storage (GCS) projects, especially those utilizing saline aquifers. The gas–liquid–solid interactions manifest in the interfacial tensions (IFTs) and contact angle determine the injectability, sealing capacity, and storage security of the GCS process. Dissolution of CO_2 in the reservoir brine occurs throughout the entire GCS process, leading to enhanced storage capacity but also to acidification of the brine, possibly leading to reservoir or seal damage. Two of the most important thermodynamic properties of the fluids are the mutual solubility and the IFT of the CO_2–brine pseudo-binary system. In this work, we report a new correlative model for the IFT between CO_2- and water-rich phases over wide ranges of temperature (273 to 473 K) and pressure (up to 100 MPa). The model is parameterized for brines comprising any combinations of sodium, potassium, calcium and magnesium cations with chloride, sulphate and bicarbonate anions up to a total molality of at least 5 mol·kg^{-1}. The independent variables in this new model are reduced temperature, ion molalities and the mole fraction of CO_2 dissolved in the aqueous phase. The latter is related to temperature, pressure and ion molalities by an improved model for the mutual solubility. More than 2000 experimental data points were used in the development of the two models. For the IFT of the CO_2-H_2O binary system, the overall root-mean-square deviation (RMSD) is 0.65 mN·m^{-1} while the absolute average relative deviation (AARD) is 1.8%. In the case of mutual solubility, the RMSD of CO_2 mole fraction in the aqueous phase is 0.0003 and the AARD is 5.5% while, in the non-aqueous phase, the RMSD of H_2O mole fraction is 0.0035 and the corresponding AARD is 8.7%. Similar results are found for the CO_2-brine systems.

1. Introduction

Despite the global effort to reduce carbon emissions since the 'Paris Treaty', greenhouse gas emissions remain unsustainably high [1,2]. The development of renewable energy and implementation of carbon capture and storage (CCS) in power generation and other industries are recognized as key to curtailing CO_2 emissions [3]. In the context of the latter, fundamental research on thermodynamic properties related to geological carbon storage (GCS) are essential in the design and optimization of this process.

Residual trapping, also known as capillary trapping, is one of the main trapping mechanisms in the GCS process (the others being structural, solubility, and mineralization trapping) [4]. The efficiency of residual trapping is determined by the threshold capillary pressure p_c^{th}, which in turn is a function of reservoir wettability and the interfacial tension (IFT) between CO_2 and reservoir brines [5]. This threshold capillary pressure characterizes the penetrating ability of the non-wetting phase (CO_2) into the macropores and throats of the reservoir rock that are originally brine saturated. The CO_2 injection pressure must exceed the threshold capillary pressure of the storage formation, to ensure displacement of brine, but be less than the threshold capillary pressure of the caprocks, to ensure storage security. This quantity can be modelled using the Young–Laplace equation for cylindrical pores of radius R:

$$p_c^{th} = p_{CO_2} - p_{brine} = \frac{2\gamma\cos\theta}{R} \quad (1)$$

Here, θ is the contact angle between the brine and rock, and γ is the

* Corresponding author.
E-mail address: m.trusler@imperial.ac.uk (J.P. Martin Trusler).

https://doi.org/10.1016/j.fuel.2023.129712
Received 11 June 2023; Received in revised form 15 August 2023; Accepted 3 September 2023
Available online 8 September 2023
0016-2361/© 2023 The Authors. Published by Elsevier Ltd. This is an open access article under the CC BY license (http://creativecommons.org/licenses/by/4.0/).

IFT between the brine and CO_2. Quantitative understanding the IFT between CO_2 and reservoir brine is essential for the design of GCS processes including quantifying residual trapping capacity and assessing caprock integrity.

In GCS, injected CO_2 dissolves into reservoir brine, leading to an increase in the density of the brine and a fluid density gradient within the formation. This eventually leads to convective mixing which enhances the dissolution rate of CO_2, leading to a substantial degree of CO_2 solubility trapping [6]. This solubility trapping mechanism plays an important role in the GCS process. Moreover, the mutual solubility between CO_2 and reservoir brine influences the long-term storage security, as well as the physical and chemical interactions between fluids and minerals within the formation [7]. To quantify these effects, it is essential to have reliable model to predict the mutual solubility between CO_2 and reservoir brines at under GCS conditions.

The (CO_2 + H_2O) binary system presents type III phase behavior according to the classification of Scott and van Konynenburg [24]. Vapor–liquid criticality exists along two loci: one starting from the critical point of pure water at $T_{c,2}$ = 647.10 K and $p_{c,2}$ = 22.064 MPa extending to indefinitely high pressures; and a second locus starting from the critical point of pure CO_2 at $T_{c,1}$ = 304.13 K and $p_{c,1}$ = 7.377 MPa, ending at the upper critical end point at T_{UCEP} = 304.63 K and p = 7.411 MPa [25]. The binary system exhibits three–phase vapor–liquid–liquid equilibrium along a curve extending from $T = T_{UCEP}$ down to the four–phase hydrate–vapor–liquid–liquid quadruple point at T_Q = 282.91 K and p_Q = 4.460 MPa [25]. At pressures below this curve and above the vapor pressure of pure water, CO_2–rich vapor and H_2O–rich liquid coexist, while above the three–phase curve a CO_2–rich liquid phase coexists with H_2O–rich liquid. A metastable vapor–liquid–liquid coexistence curve persists at temperatures from T_Q down to the triple–point temperature of water at 273.16 K [25]. Thus, it is possible to measure and model the mutual solubility and IFT of CO_2 and H_2O at temperatures down to the melting curve of water at a given pressure.

Several researchers have reviewed and analyzed experimental solubility data for the CO_2 + H_2O systems with a view to establishing reliable empirical correlations of the Henry's law constant [26,27] eventually leading to a reliable formulation valid in a wide range of temperatures up to the critical point of water [28]. Experimental solubility data for the CO_2 + H_2O system were compiled and tabulated in the 1996 Solubility Series of the International Union of Pure and Applied Chemistry (IUPAC) [29] and a large amount of additional data have been published since; see section 2 for a review of the available data.

As detailed in Table 1, numerous model have been proposed in the literature to represent the mutual solubility of the (CO_2 + H_2O) system or for computing the composition of one phase or the other under saturated conditions. These models include application of an equation of state (EoS) to both phase (φ–φ approach), use of an activity–coefficient model for the aqueous phase and an EoS for the CO_2–rich phase (γ–φ approach), the Krichevsky–Kasarnovsky (extended Henry's law) approach [9] and empirical equations. A machine learning technique has also been demonstrated [30].

The importance of these models is that some of them provide a basis for the development of a wide-ranging model for CO_2–brine systems. The φ–φ approach with cubic EoS (cEoS) implemented with traditional van der Waals mixing rules is not generally suitable for representing the mutual solubility but may be tuned to represent either the CO_2 solubility in the aqueous phase or the H_2O content of the non–aqueous phase at saturation [20]. This limitation arises from the very different nature of the phases. Much improved results can be obtained with cEoS by using non–conventional mixing and combining rules that emulate an activity coefficient model in the liquid phase; examples include the Wong-Sandler method [31]. More complex EoS models such as the CPA equation [32,33] and various version of the SAFT approach [18,34] yield generally improved results when tuned specifically to experimental data for the CO_2–H_2O system. This success is attributed to explicit modelling of the hydrogen–bonding association between water molecules and, in some implementations, to cross association between CO_2 and H_2O [33]. The φ–φ approach can be extended to CO_2–brine systems accurately, for example by using a cEoS with non–conventional mixing rules incorporating an electrolyte activity model. Unfortunately, this leads to a rather complex model. Generally, γ–φ approaches have been the most successful at the temperatures of interest in GCS [9,15,21]. They can describe the compositions of both phases accurately and are capable of systematic extension to incorporate salt effects [21]. Such models fail as one approaches the critical temperature of the solvent but this is not a limitation for CGS applications. The KK approach can be viewed either as a simplification of the γ–φ approach or as an extension of Henry's law aimed at representing the solubility of CO_2 in the aqueous phase [21]. In this approach, the fugacity of the CO_2 in the non–aqueous phase is modelled by treating that phase as an ideal mixture of non–ideal gases, while the fugacity of the CO_2 in the aqueous phase is modelled by a Henry's constant, depending upon temperature, and a Poynting correction estimated at a function of temperature and pressure from the partial molar volume of the CO_2 at infinite dilution. In the CO_2–H_2O system, it was found to perform poorly at temperatures above 373 K [21] and it is also not suitable for representing accurately the H_2O content of the non–aqueous phase.

Table 2 summarizes the models reported in the literature for CO_2–brine systems. Strong electrolytes have a salting–out effect, lowering the solubility of CO_2 relative to that in pure water at the same

Table 1
Literature models for CO_2-H_2O mutual solubility (EoS denotes equation of state and ACM denotes activity coefficient model).

First Author, Year	Method	Phases	EoS	ACM	T/K	p_{max}/ MPa
Coan, 1971 [8]	γ–φ	G	Virial	–	298–373	6
Carroll, 1992 [9]	KK	L	RK	-	273–373	50
	γ–φ	L, G	RK	M2S		
King, 1992 [10]	KK	L, G	RK		288–313	50
Duan, 1992 [11]	φ–φ	L, G	m-BWR	–	323–1273	100
Shyu, 1996 [12]	φ–φ	L, G	m-PR-WS	–	298–623	100
Bamberger, 2000 [13]	φ–φ	L, G	m-PR-PR	–	313–353	14
Kiepe, 2002 [14]	φ–φ	L, G	PSRK	–	313–393	10
Spycher, 2003 [15]	γ–φ	L, G	m-RK-PR	Henry	285–383	60
Diamond, 2003 [16]	γ–φ	L, G	LFR	EE	273–373	10
Chapoy, 2004 [17]	φ–φ	L, G	PT		298–373	100
Valtz, 2004 [18]	γ–φ	L, G	PR	Henry	274–351	7.3
	φ–φ	L, G	PR-WS	-		
	φ–φ	L, G	SAFT	-		
Siqueira Campos, 2009 [19]	γ–φ	L	EE	UNIFAC	298–323	0.6
Tabasinejad, 2011 [20]	γ–φ	G	PR	Henry	423–478	124
	φ–φ	G	CPA	-		
Hou, 2013 [21]	γ–φ	L, G	PR	NRTL	298–448	18
Jiang, 2014 [22]			PR		333–373	18
Sarapardeh, 2020 [23]	ML	L	–	–	197–623	350

Abbreviations: BWR = Benedict-Webb-Rubin, CPA = cubic plus association, EE = Empirical equations, Henry = Henry's law, possibly with the Poynting correction, LFR = Lewis fugacity rule, M2S = Margules two suffix model, PR = Peng-Robinson, PSRK = predictive Soave-Redlich-Kwong, PT = Patel-Teja, RK = Redlich-Kwong, SAFT = Statistical Associating Fluid Theory. Prefix: m = modified. Suffixes (mixing/combining rules): WS = Wong-Sandler, PR = Panagiotopoulos-Reid, ML = Machine-learning.

Table 2
Literature models of CO_2–brine mutual solubility with maximum salt molality m_{max}, temperature range T and maximum pressure p_{max} (EoS denotes equation of state and ACM denotes activity coefficient model).

First Author, Year	Salts	Method	Phases	EoS	ACM	$\frac{m_{max}}{mol \cdot kg^{-1}}$	$\frac{T}{K}$	$\frac{p_{max}}{MPa}$
Bowers, 1983 [43]	NaCl	φ–φ	L, G	m-RK	–	5.7	273–973	200
Rumpf, 1994 [44]	NaCl	γ–φ	L	Virial	Pitzer	6	313–433	10
Duan, 1995 [45]	NaCl	φ–φ	L, G	TPT	–	1	573–973	600
Kiepe, 2002 [14]	NaCl/KCl	φ–φ	L	PSRK	–	4.34	313–353	10.5
Bando, 2003 [46]	NaCl	γ–φ	L	Ideal	Henry	0.03	313–333	20
Duan, 2003 [39]	NaCl	γ–φ	L,G	LFR	Pitzer	4.3	273–533	200
Bermejo, 2005 [47]	$NaSO_4$	φ–φ	L	AP	–	0.0125	288–368	14
Spycher, 2005 [41]	NaCl/KCl/ $CaCl_2/MgCl_2$	γ–φ	L, G	m-RK	Pitzer	6	285–373	60
Duan, 2006 [40]	NaCl/KCl/ $CaCl_2/MgCl_2$	γ–φ	L, G	EE	Pitzer	4.5	273–573	200
Spycher, 2010 [42]	NaCl/KCl/ $CaCl_2/MgCl_2$	γ–φ	L, G	m-RK	Pitzer	6	285–573	60
Yan, 2010 [48]	NaCl/Na_2SO_4	γ–φ	L	SAFT	eNRTL	2	273–473	150
Springer, 2012 [49]	NaCl/KCl/ $CaCl_2$	γ–φ	L, G	SRK	MSE	6	298–433	10.1
Hou, 2013 [50]	NaCl/KCl	γ–φ	L, G	PR	eNRTL	4	232–423	18
Bastami, 2014 [51]	$CaCl_2$	γ–φ	L,G	LFR	Pitzer	4	328–375	20.7
Parkhurst, 2013 [52] Appelo, 2014 [53] Appelo, 2015 [54]	Na–K–Mg–Ca–Cl–HCO_3 –SO_4	γ–φ	L, G	PR	Pitzer	6	273–473	101.3
Zhao, 2015[55]	$CaCl_2/MgCl_2/$ Na_2SO_4 /KCl	γ–φ	L	m-RK	Pitzer	6	323–523	150
dos Santos, 2021 [56]	NaCl/Na_2SO_4	γ–φ	L, G	PR	Pitzer	6	273–473	40
Sun, 2021 [57]	NaCl/KCl/ $CaCl_2/MgCl_2$	EE	L, G	–	–	4.29	273–523	200
Retnakar, 2023 [58]	Complex brine	ML	L	–	–	2.5	278–477	350

Abbreviations: AP = Anderko-Pitzer model, EE = empirical equation, eNRTL = Electrolyte NRTL model, Henry = Henry's law, possibly with Poynting correction, LFR = Lewis fugacity rule, Pitzer = Pitzer-Debye-Hückle model (or simplification thereof) with Henry's law, PR = Peng-Robinson, RK = Redlich-Kwong, SAFT = Statistical Associating Fluid Theory, SRK = Soave-Redlich-Kwong, TPT = Thermodynamic perturbation theory, ML = Machine-learning. Prefix: m = modified.

temperature and pressure. Often, these effects are accounted for by means of an electrolyte activity coefficient model within an overall γ–φ approach. The Pitzer model is widely used in this context, and is applicable to both ionic and molecular species in solution over a broad range of ionic strengths up to 20 $mol \cdot kg^{-1}$ [35–38]. The solubility model of Duan et al. [39] for the CO_2 + brine binary system combined an equation of state for the non–aqueous phase with a simplified Pitzer–type model to account for the cations Na^+, K^+, Mg^{2+}, Ca^{2+} and anions Cl^-, SO_4^{2-}, HCO_3^- and CO_3^{2-}. This model was stated to be valid for temperatures from 273 K to 533 K and pressures up to 200 MPa with NaCl molality up to 4.5 $mol \cdot kg^{-1}$. In later work [40], the EoS was replaced by empirical equations that avoid the need for iterations, and the accuracy of the prediction model was improved for $T < 288$ K. Unfortunately, the models of Duan et al. [39,40] were not intended to compute the solubility of H_2O in the compressed CO_2–rich phase. Spycher and Pruess [15,41,42] evolved a model for the mutual solubility of the CO_2–brine system. This work started with the CO_2–H_2O system at temperatures up to 373 K [15]; next salt effects were included [41]; and finally, the temperatures range was extended up to 573 K to allow application to both CGS and enhanced geothermal systems [42]. Overall, the model adopts a γ–φ approach with a modified Redlich–Kwong EoS for the CO_2–rich phase and a combination of a Margules equation and a simplified Pitzer–type model for the activity coefficients in the aqueous phase. Despite generally good performance, the model suffers from the use of separate mathematical formulations below and above 373 K and it does not distinguish between Na^+ and K^+ and between Ca^{2+} and Mg^{2+}. More recently, Sun et. al. [57] have proposed a model for the prediction of mutual solubility in CO_2–brine systems containing a variety of ions. This model is wide ranging and exhibits generally good agreement with experiment; however, it is empirical in nature. Generally, the effect of strong electrolytes is quite easy to model either with an activity coefficient approach or via Setchenov coefficients [59].

Abundant experimental data are available on the IFT between CO_2 and water or brine, covering temperatures of 278 K to 473 K with pressures up to 70 MPa, with a few data available at higher pressures. A notable feature is that strong electrolytes typically raise the IFT relative to the CO_2 + H_2O system in a manner that does not vary rapidly with temperature or pressure. The experimental data are reviewed section 3 of this article. Table 3 summarizes previous modelling approaches for the IFT between CO_2 and water or brine [60–73]. These fall into four main categories: molecular simulation, density gradient theory, empirical correlation and artificial neural network models. Molecular dynamics simulations can yield impressive results but are computationally intensive. The density gradient theory, coupled with an equation of state, is less computationally demanding but still too slow for routine calculations. It also requires so-called influence parameters which can be estimated from pure-component surface tension but only for sub-critical components. This presents a problem for supercritical CO_2 which has been addressed in various ways in the literature [63,66,68]. Empirical models have been used by several authors, sometime piecewise to handle both sub- and super-critical conditions [64,67,73]. Kashefi [64] noted that the IFT of the CO_2 + H_2O system correlated with CO_2 solubility, even across phase boundaries, reducing to the water surface tension at zero CO_2 mole fraction. It was also noted that a similar approach applied to CO_2 + brine solutions. Artificial neural network models have also been quite successful in describing CO_2-water/brine IFT. All of these approaches have merit but it can be observed that the simplest and often most accurate descriptions have been mainly empirical.

For both the IFT and the mutual solubility of CO_2 + brine systems, one can note that an accurate model for the CO_2 + H_2O binary system is a pre-requisite and that accounting for salt effect is then relatively straight-forward. In this study, we set out to develop an accurate, wide–ranging and computationally–efficient model for the CO_2–brine IFT that would be applicable to a wide range of brine chemistry and at temperatures and pressures relevant to GCS conditions. In constructing this, we found it useful to relate the IFT to the solubility of CO_2 in the brine and, for that purpose, developed an improved model for the

Table 3
Literature models for CO_2–brine IFT.

First Author, Year	Salts	Method	m_{max} / mol·kg^{-1}	T/K	p_{max} / MPa
Rocha, 2001 [60]		MD	0	318–338	28
Kuznetsov, 2002 [61]		MD	0	285–298	30
Nielsen, 2012 [62]		MD	0	298–383	40
Georgiadis, 2010 [63]		DGT + SAFT-VR	0	298–374	60
Kashefi, 2012 [64]		EE	0	284–398	44
Li, 2013 [65]	$CaCl_2$	MD	5	303–393	50
Khosharay, 2014 [66]		DGT + PC-SAFT	0	298–398	60
Chow, 2016 [67]		EE	0	298–448	40
Chow, 2016 [68]		DGT + SAFT-VR	0	298–473	60
Partovi, 2017 [69]	NaCl/KCl/Na_2SO_4 /$MgCl_2$/$CaCl_2$	ANN	5	278–448	60
Che Ruslan, 2018 [70]	NaCl/KCl/$CaCl_2$	DGT + CPA	5	298–443	70
Liu, 2021 [71]	NaCl	ANN	5	293–433	20
Song, 2020 [72]	NaCl	ANN	10	273–310	14
Jerauld, 2022 [73]	NaCl/KCl/$CaCl_2$ $MgCl_2$/Na_2SO_4	EE	5	298–478	60
Amooie, 2019 [74]	Complex brine	ML	5	298–423	50

ANN = Artificial neural network, DGT = Density gradient theory, MD = Molecular dynamics, EE = Empirical equations, SAFT = Statistical associating fluid theory equation of state, CPA = cubic plus association equation of state. Prefix: PC = perturbed hard-chain. Suffix: VR = variable range, ML = Machine-learning.

mutual solubility. The new models are intended to address the shortcomings of earlier work through careful model construction designed to achieve low uncertainties while retaining a sufficient simplicity for application in e.g. large–scale reservoir simulations that require very large number so function evaluations. Considering the available data, we have parameterized the model for the temperature range of 273 K to 473 K and for pressures up to 100 MPa. The model is designed for brines containing cations Na^+, K^+, Mg^{2+}, Ca^{2+} and anions Cl^-, SO_4^{2-}, HCO_3^- and CO_3^{2-} with a total salt molality up to 5 mol·kg^{-1}.

2. Solubility model

The mutual solubility model presented in this work is based on the 'γ–φ' approach in which an activity–coefficient model is used to describe non–ideality in the aqueous phase and an equation of state is used for the non–aqueous phase. The approach is similar to that of Spycher and Pruess [15,42] with significant changes adopted to satisfy the following objectives:

- Use of a single set of equations and parameters to cover the temperature range from 273.15 K to 473.15 K with pressures up to 100 MPa
- Key pure–component and partial–molar quantities calculated from well–established independent correlations
- Interaction parameters optimized against an extended data set including recent results for the solubility of CO_2 in water and different brines.

2.1. Model structure

In the 'γ–φ' approach, phase equilibrium of a binary solute–solvent system can be expressed exactly by the following pair of equations:

$$y_1\varphi_1 p = x_1\gamma_1 H_{12}\exp\left[\int_{p_2^{sat}}^{p}(V_1/RT)dp\right] \tag{2}$$

$$y_2\varphi_2 p = x_2\gamma_2\left(\varphi_2^{sat}p_2^{sat}\right)\exp\left[\int_{p_2^{sat}}^{p}(V_2/RT)dp\right] \tag{3}$$

Here, component 1 is the solute (CO_2) and component 2 is the solvent (H_2O); y_i and φ_i are the mole fraction and fugacity coefficient of component i in the non–aqueous phase; x_i and γ_i are the mole fraction and activity coefficient of component i in the aqueous phase; H_{12} is Henry's constant, p is pressure and V_i are partial molar volumes in the aqueous phase; finally superscript 'sat' denotes properties of pure saturated solvent. In this formulation, activity coefficients are defined in the asymmetric convention ($\gamma_2 \to 1$ as $x_1 \to 0$) and are functions of temperature and composition only. Henry's constant is defined on a mole–fraction basis, has the same dimensions as pressure and is a function of temperature only. Fugacity coefficients in the non–aqueous phase (gas, liquid or supercritical) are evaluated from an equation of state, while activity coefficients in the aqueous phase are evaluated from an activity–coefficient model.

Generally, the partial molar volumes are function of temperature, pressure and composition. However, for a sparingly–soluble solute in a low–compressibility solvent, such as the CO_2–H_2O system, one can approximate V_1 by the partial molar volume of the solute evaluated at infinite dilution and at $p = p_2^{sat}$, which we denote V_1^{∞}, and approximate V_2 by the molar volume of the pure saturated solvent V_2^{sat}. The phase equilibrium conditions may then be conveniently written as

$$y_1\varphi_1 p = x_1\gamma_1 K_1 \tag{4}$$

$$y_2\varphi_2 p = x_2\gamma_2 K_2 \tag{5}$$

where the K_i are equilibrium constants given by

$$K_1 = H_{12}\exp\left[V_1^{\infty}(p - p_2^{sat})/RT\right] \tag{6}$$

$$K_2 = \left(\varphi_2^{sat}p_2^{sat}\right)\exp\left[V_2^{sat}(p - p_2^{sat})/RT\right] \tag{7}$$

which both have the dimensions of pressure. In this work, the only parameters adjusted to fit the experimental phase–equilibrium data for CO_2 + H_2O are those within the equation of state and activity–coefficient models, as discussed further below. The equilibrium constants are fully determined by well–established independent models.

When salt is present in the aqueous phase (only), the basic formulation of the model remains the same but the activity coefficients in the liquid phase become functions of both the CO_2 and ion concentrations. The presence of ionic solutes of course impacts the calculation of the mole fractions of CO_2 and H_2O in the aqueous phase. Assuming that the salts are fully dissociate in the aqueous phase and absent from the non–aqueous phase, the solution of the problem for x_1 and y_2 at given T, p, and ion molalities is given by [41]

$$y_2 = \frac{(1-B)}{(1/A - B)(1 + m_s M_2) + B m_s M_2} \tag{8}$$

$$x_1 = B(1 - y_2) \tag{9}$$

Here, $M_2 = 0.018015$ kg•mol^{-1} is the molar mass of water, m_s is the sum of all ion molalities and A and B are dimensionless parameters given by

$$A = \frac{\gamma_2 K_2}{\varphi_2 p} \tag{10}$$

$$B = \frac{\varphi_1 p}{\gamma_1 K_1} \tag{11}$$

The molality m_1 of CO_2 in the aqueous phase may also be calculated as

$$m_1 = x_1\left(m_s + M_w^{-1}\right)/(1 - x_1) \tag{12}$$

The solution is developed by iterations because the fugacity coefficients and activity coefficients depend upon composition.

2.2. Equilibrium constants

For Henry's constant of CO_2 in water, we adopt the correlation of Fernandez–Prini at al. [28] which is based on a critical review of the available data and is applicable up to the critical point of water. The properties of pure saturated water (p_2^{sat}, φ_2^{sat} and V_2^{sat}) are evaluated from the IAPWS–95 equation of state for water [75]. The partial molar volume of CO_2 at infinite dilution in aqueous solution is determined from the correlation of McBride–Wright et al. [76] evaluated at $p = p_2^{sat}$; this is in good agreement with the model of Sedlbauer et al. [77]. These models may be applied directly in their original forms. However, solely for simplicity of application, we provide polynomial approximations for the required properties, as follows:

$$\ln(H_{12}/\mathrm{MPa}) = \sum_{i=0}^{3} a_i \tau^i \tag{13}$$

$$\ln\left(\varphi_2^{sat} p_2^{sat}/\mathrm{MPa}\right) = \sum_{i=0}^{3} b_i \tau^i \tag{14}$$

$$V_2^{sat}/(\mathrm{cm}^3\cdot\mathrm{mol}^{-1}) = \sum_{i=0}^{3} c_i \tau^i \tag{15}$$

$$V_1^{\infty}/(\mathrm{cm}^3\cdot\mathrm{mol}^{-1}) = \sum_{i=0}^{3} d_i \tau^i \tag{16}$$

Here, $\tau = (T/T_{UCEP}) - 1$ is a dimensionless reduced temperature ($T_{UCEP} = 304.63$ K). The coefficients are given in Table 4 along with the root–mean–square deviations σ between the polynomial approximations and the original models for the dimensionless quantities as defined in Eqs. (13)–(16) at temperatures between 273.15 K and 473.15 K. The differences between the polynomial approximations and the original models are insignificant in the present context.

Table 4
Coefficients in equations (13) to (16).

	$i = 0$	$i = 1$	$i = 2$	$i = 3$	$i = 4$	σ
a_i	5.2677	7.1625	–16.3072	17.4946	–9.0997	0.0015
b_i	–5.3804	17.3049	–19.6272	17.4627	–8.4245	0.0014
c_i	18.1040	1.6946	7.3717	–6.9088	7.5670	0.0015
d_i	34.3287	13.7101	30.4981	0.8212	–2.3406	0.0005

2.3. Equation of state

In this work, we use the Peng–Robinson equation of state (PR-EoS) to evaluate the fugacity coefficients of CO_2 and H_2O in the non–aqueous phase (vapor, liquid or supercritical). This equation of state is simple, widely used and easily applied to mixtures by invoking standard one–-fluid mixing rules as detailed in Appendix A. However, cubic equations of state, such as the PR-EoS, coupled with conventional one-fluid mixing and combining rules can be inaccurate for mixtures of water and non-polar molecules such as CO_2. Therefore, we follow Spycher and Pruess [42] in adopting the unconventional combining rule of Panagiotopoulos and Reid [78], as reformulated in Orbey and Sandler [79], for the unlike attractive parameter a_{ij} (see A**ppendix A):

$$a_{ij} = \sqrt{a_i a_j}\left[1 - k_{ij} + \left(k_{ij} - k_{ji}\right)y_i\right] \tag{17}$$

This approach allows a_{ij} to vary with composition. Furthermore, the binary interaction parameters k_{12} and k_{21} are expressed as linear functions of reduced temperature as follows:

$$k_{ij} = k_{ij,0} + k_{ij,1}\tau \tag{18}$$

Based on these mixing and combining rules, the fugacity coefficient of component k in the non–aqueous phase is given by [79]:

$$\ln(\phi_k) = \frac{B_k}{B}(Z-1) - \ln(Z-B) + \frac{A}{2\sqrt{2}B}\left[\frac{B_k}{B} - \left(\frac{\sum_i y_i(a_{ik}+a_{ki}) - \sum_i\sum_j y_i^2 y_j (k_{ij}-k_{ji})\sqrt{a_i a_j} + y_k \sum_i y_i (k_{ki}-k_{ik})\sqrt{a_i a_k}}{a}\right)\right] \times \ln\left[\frac{Z + (1+\sqrt{2})B}{Z + (1-\sqrt{2})B}\right], \tag{19}$$

where Z is the compressibility factor and other parameters are defined in Appendix A.

2.4. Activity coefficient model

The activity coefficients are given by a modified version of the Margules expression

$$\ln(\gamma_1) = 2Ax_1x_2^2 + \ln(\gamma_1') \tag{20}$$

$$\ln(\gamma_2) = A(1-2x_2)x_1^2 \tag{21}$$

where A is a function of temperature and γ_1' is a factor that accounts for the salt effect on the activity coefficient of CO_2 in saline solutions. In this work, we represent A by the following quadratic function of reduced temperature τ:

$$A = A_0 + A_1\tau + A_2\tau^2 \tag{22}$$

The salt term was adapter from Spycher and Pruess [42] as follows:

$$\ln(\gamma_1') = \ln(1 + m_s M_2) + 2\lambda\left(\delta_1 m_{Na} + \delta_2 m_K + \delta_3 m_{Mg} + \delta_4 m_{Ca}\right) + \xi m_{Cl}\left(m_{Na} + m_K + m_{Mg} + m_{Ca}\right) + \delta_5 m_{SO_4} + \delta_6 m_{HCO_3}, \tag{23}$$

where m_X denotes molality of ion X and λ and ξ are given as functions of reduced temperature by

Table 5
Literature data for CO_2–H_2O mutual solubility. [1]

Source	T/K	p/MPa	N_{aq}	N_{non-aq}
Al Ghafri, S. 2014 [81]	323	2.0–18.7	8/8	
Anderson,G.K., 2002 [82]	274–288	0.07–2.2	54/54	
Bamberger,A., 2000 [13]	323–353	4.0–14.2	29/29	29/29
Bando,S., 2003 [46]	313–333	10–20	9/9	
Bastami,A., 2014 [51]	328–375	6.8–20.7	10/10	
Chapoy,A., 2004 [17]	274–351	0.2–7.31	27/27	
Dalmolin,I., 2006 [83]	288–323	0.1–0.5	49	
Dell'Era,C., 2010 [84]	298–299	0.2–0.8	7	
Ferrentino,G., 2010 [85]	308–323	5.5–15.0	0/22	
Foltran,S., 2015 [86]	313	8.0–12.5		0/5
Han,J.M, 2009 [87]	313–343	4.3–17.3	28/28	
Hou,S.X., 2013 [21]	298–448.	1–18	38/38	38/37
Iwai, 2004 [88]	313	15		0/1
Jiang, C.Y., 2014 [22]	333–373	8–18		10/20
Kiepe,J., 2002 [89]	313–393	0.1–10.0	0/40	
Krotov,D., 2014 [90]	353	0.6–9.7	0/5	
Liu,Y., 2011 [91]	308–323	2–16	31/31	
Liu,Y., 2012 [92]	308–318	8–16	6/6	
Martin,A., 2009 [93]	353–393	10–30	5/5	5/5
Meyer,C.W., 2015 [94]	283–333	0–5		58/58
Muromachi,S., 2015 [95]	286–298	0.2–4.0	17/17	
Qin,J., 2008 [96]	323–324	0.03–0.05	0/2	
Ruffine,L., 2010 [97]	333	4.8–11.5	3/3	
Schüler, N., 2012 [98]	308–333	0.1	0/7	
Serpa,F.S., 2013 [99]	298–323	0.1–0.4	9/9	
Servio, P., 2001 [100]	278–283	2.0–3.7	6/6	
Siqueira Campos,C.E.P, 2009 [19]	298–323	0.05–0.60	50/50	
Tabasinejad,F., 2011 [20]	423–478	4–103		35/35
Tang,Y., 2015 [101]	308–468	8–41	14/27	
Tong,D., 2013 [102]	374–323	7–27	5/5	
Valtz, 2004 [18]	278–318	0–8	40/47	60/60
Wang,Z., 201 3[103]	313–373	9–18		4/4
Zhang,G, 2005 [104]	304–313	1.0–4.6	8/8	

[1] N_{aq} is the number of aqueous phase data points used/reported; N_{non-aq} is the number of non–aqueous phase data points used/reported.

Table 6
Literature data for CO_2 solubility in brines. [1]

Authors	Salt	T/K	p/MPa	m/(mol·kg^{-1})	N_{aq}
Koschel (2006) [105]	NaCl	323–373	5–20	1–3	14/14
Kiepe (2002) [89]	NaCl	313–352	0.1–10	0.5–4.3	61/64
Rumpf (1994) [44]	NaCl	313–433	0.5–9.6	4–6	63/63
Nighswander (1989) [106]	NaCl	353–433	2–10	0.18	25/24
Hou et al. (2013) [50]	NaCl	323–423	2.6–18.2	2.5–4.0	36/36
Guo et al. (2016) [107]	NaCl	273–453	10–40	1–5	167/168
Bando (2003) [46]	NaCl	303–333	10–20	0.18–0.55	36/36
Zhao et al. (2015) [108]	KCl	323–423	15	0.5–4.5	18/18
Kiepe (2002) [89]	KCl	313–353	0.1–10.5	0.5–4.0	0/86
Hou et al (2013) [50]	KCl	323–423	2.7–18.2	2.5–4.0	35/35
Zhao et al. (2015) [108]	$MgCl_2$	323–423	15	0.3–2.0	17/17
dos Santos (2021) [109]	$MgCl_2$	323–423	1.6–20.3	1–5	32/32
Tong et al. (2013) [102]	$MgCl_2$	310–425	1.2–34.9	1–5	39/39
Zhao et al. (2015) [108]	$CaCl_2$	323–423	15	0.3–2.0	18/18
Tong et al. (2013) [102]	$CaCl_2$	310–425	1.5–38.0	1–5	35/35
Zhao et al. (2015) [108]	Na_2SO_4	323–423	15	0.3–2.0	17/17
Han et al. (2011) [110]	$NaHCO_3$	313–333	0.3–2.0	0.1–1.0	44/44
Hoballah (2017) [80]	$NaHCO_3$	348–398	5–50	0.8	12/12

$$\lambda = 0.06754(\tau+1) + 0.00353/(\tau+1) + 0.02854/(\tau+1)^2 \quad (24)$$

$$\xi = 0.00396(\tau+1) - 0.06605/(\tau+1) + 0.05667/(\tau+1)^2 \quad (25)$$

In the model of Spycher and Pruess [42], $\delta_1 = \delta_2 = 1$, $\delta_3 = \delta_4 = 2$, $\delta_5 = -0.07$ and $\delta_6 = 0$. Hoballah [80], included the additional term for the bicarbonate ion with $\delta_6 = -0.0836$, based on his CO_2 solubility measurements in $NaHCO_3$(aq) at a molality of 0.8 mol·kg^{-1}. In this work, we have evaluated the available CO_2 solubility in single–salt saline solutions based on each coefficient δ_i being a linear function of reduced temperature:

$$\delta_i = \delta_{i,0} + \delta_{i,1}\tau \quad (26)$$

2.5. Experimental data

Table 5 details the experimental data used in the parameterization of the model for the CO_2 + H_2O binary system. The assembled database contained 549 measurements of CO_2 solubility in the aqueous phase and 255 measurements of H_2O solubility in the non–aqueous phase covering temperatures from 273.15 K to 448.15 K with pressures up to about 40 MPa. Table 6 details the data used for saline solutions. In this case, only CO_2 solubilities in the aqueous phase were analyzed.

2.6. Parameter adjustment

For the CO_2 + H_2O binary system, the goodness of fit was measured by objective functions defined as follows:

$$\left.\begin{aligned}\chi_1^2 &= \sum_i \left(x_{1,i}^{exp} - x_{1,i}^{calc}\right)^2 \\ \chi_2^2 &= \sum_i \left(y_{2,i}^{exp} - y_{2,i}^{calc}\right)^2\end{aligned}\right\} \quad (27)$$

where superscripts 'exp' and 'calc' denote experimental and calculated values at the i^{th} state point. Considering the number and magnitude of the available data in each phase, the overall objective function adopted for the final fitting was

$$\chi^2_{\text{non - saline}} = \sum_i \left(x_{1,i}^{exp} - x_{1,i}^{calc}\right)^2 + 0.1\sum_i \left(y_{2,i}^{exp} - y_{2,i}^{calc}\right)^2 \quad (28)$$

The seven parameters to be adjusted for the binary system were the four unlike $k_{ij,l}$ parameters in eq. (18) and the three A_i parameters in eq. (22). After some trial fitting, a small proportion of the available data were identified as outliers and excluded from further consideration. The number of excluded data points can be deduced from Table 5 which lists, for each data set and phase, the number of points used in the fit and the total number reported in the original publication. All parameters were found to influence the objective function to the extent that omitting any one term would increase χ^2 for one phase or the other by 10% or more. The greatest sensitivity was observed for the parameter $k_{21,1}$ which largely determines the unlike term in the PR-EoS for CO_2-rich phase. Fits in which the Margules parameter A was treated as either a constant or a linear function of temperature were also trialed, but it was verified both that the quadratic form provided a significantly better fit and that additional polynomial terms did not further improve the fit. Furthermore, making the binary-interaction parameters in the PR EoS quadratic function of temperature led to no significant improvement. Table 7 lists the goodness–of–fit metrics for the new model in comparison with the

Table 7
Objective functions for the CO_2 + H_2O system.

Objective function	This work	Spycher and Pruess [42]	Duan [40]
$\chi^2_{CO_2}$	1.1×10^{-4}	2.4×10^{-4}	2.77×10^{-4}
$\chi^2_{H_2O}$	2.9×10^{-3}	13.1×10^{-3}	13.4×10^{-3}
$\chi^2_{\text{non - saline}}$	4.1×10^{-4}	15.4×10^{-4}	16.2×10^{-4}

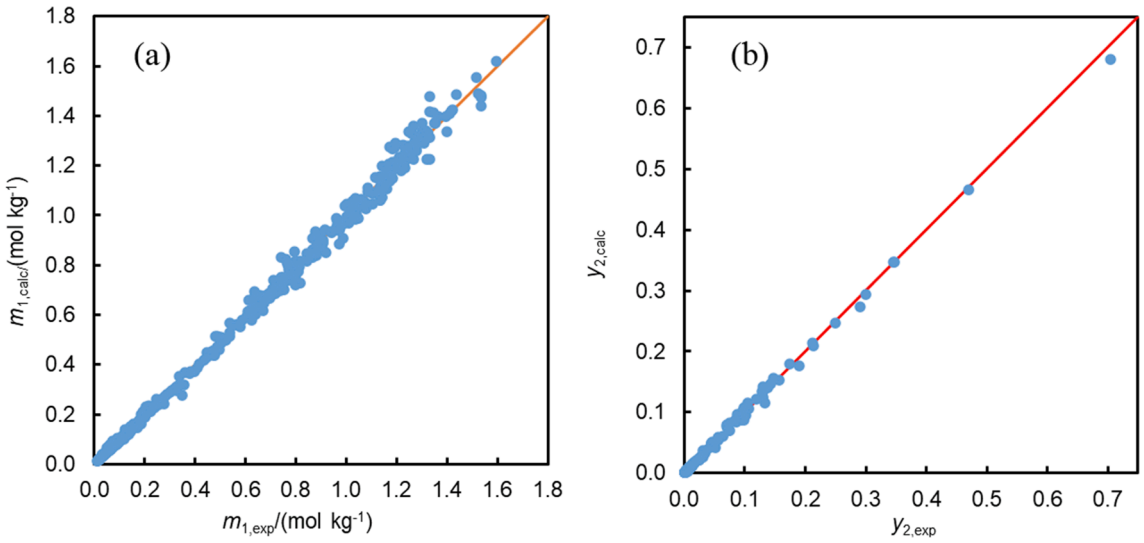


Fig. 1. Parity plots for the $CO_2 + H_2O$ binary system showing: (a) calculated molalities $m_{1,calc}$ of CO_2 in the aqueous phase against experimental values $m_{1,exp}$; and (b) calculated mole fractions $y_{2,calc}$ of H_2O in the non–aqueous phase against experimental values $y_{2,exp}$.

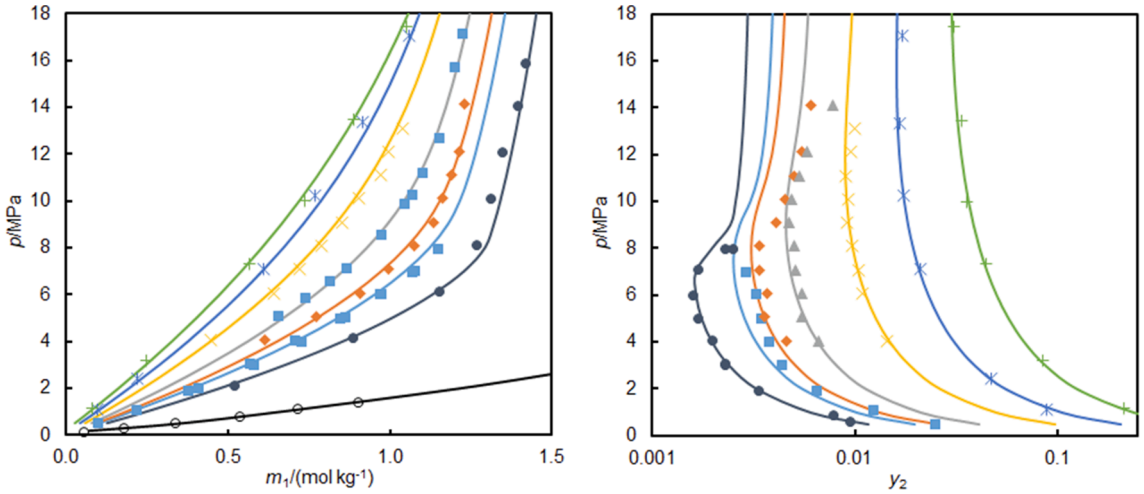


Fig. 2. Comparison between predicted and experimental mutual solubility. Symbols represent experimental data and curves are calculated from the model. (a) Pressure p plotted against molality m_1 of CO_2 in the aqueous phase: ●, $T = 308.15$ K, [91]; ■, $T = 318.23$ K, [18]; ◆, $T = 323.2$ K [13]; △, $T = 333.2$ K [87]; ×, $T = 353.1$ K [13]; *, $T = 373.15$ K [21]; +, $T = 398.15$ K [21]. (b) Pressure p plotted against mole fraction y_2 of water in the non-aqueous phase: ●, $T = 308.15$ K [18]; ■, $T = 318.23$ K [18]; ◆, $T = 323.2$ K [13]; △, $T = 333.2$ K [13]; ×, $T = 353.1$ K [13]; *, $T = 373.15$ K SPS:refid::bib21[21]; +, $T = 398.15$ K [21].

models of Spycher and Pruess [42] and Duan [40] for the same data set. One can observe a significant improvement in the representation of both the aqueous phase and non–aqueous phases. This has been achieved in part by restricting the temperature range of the model to those of interest in CGS and in part by refinement of the experimental data set used in the fitting.

Fig. 1 (a) is a parity diagram comparing the experimental and calculated solubilities of CO_2 in the aqueous phase of the $CO_2 + H_2O$ binary system, expressed in terms of molality. The data are well represented with an overall root–mean–square molality deviation of 0.029 mol·kg^{-1}. In terms of the CO_2 mole fraction in the aqueous phase, the root mean squared deviation (RMSD) is 0.0003, while the absolute average relative deviation (AARD) is 5.5%. Fig. 1 (b) shows a similar parity diagram for the mole fraction of H_2O in the non–aqueous phase. In this case, the overall RMSD for mole fraction is 0.0035 and the AARD is 8.7%. Fig. 2 shows a comparison between the model predictions and a representative set of literature data along isotherms. The agreement between the model and experiment is generally good, although the model does not fully capture the shape of $p(y_2)$ at low temperatures where the water mole fraction along an isotherm passes through a minimum.

For the saline solutions, molality is preferred as the measure of composition and the objective function aqueous–phase composition only, was:

$$\chi^2_{saline} = \sum_i \left(m^{exp}_{1,i} - m^{calc}_{1,i} \right)^2 \quad (29)$$

Fig. 3 shows a set of parity plots comparing the model predictions with experiment for six different brine chemistries. Again, good agreement is observed. The full set of parameters obtained by the analysis of non–saline and saline systems is listed in Table 8.

3. Interfacial tension model

3.1. Model structure

As discussed in the introduction, the ($CO_2 + H_2O$) binary system can exhibit three–phase vapor–liquid–liquid coexistence (either metastable

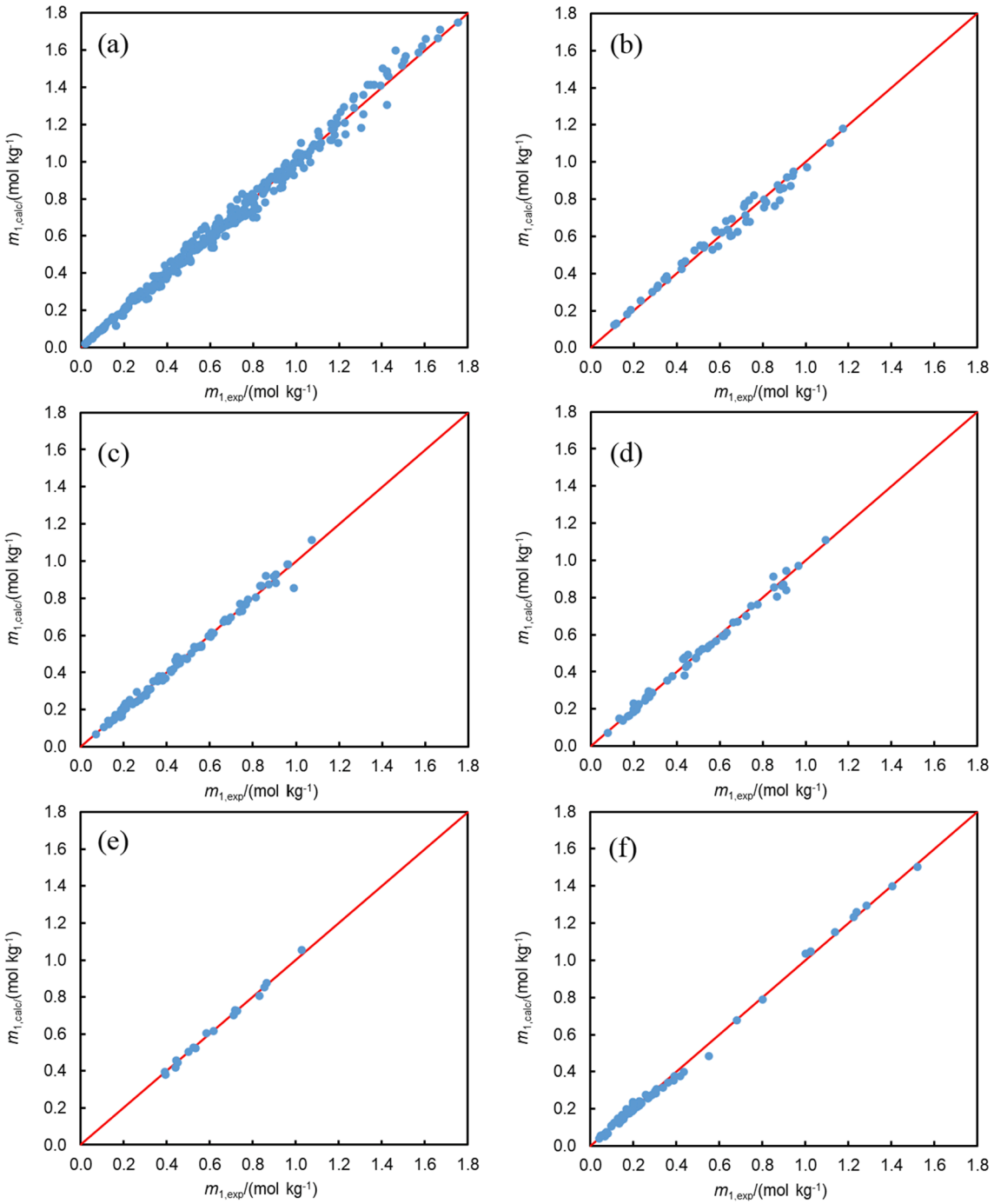


Fig. 3. Parity plots for the CO_2 solubility in the aqueous phase of saline solutions showing calculated molalities $m_{1,calc}$ of CO_2 in the aqueous phase against experimental values $m_{1,exp}$: (a) NaCl(aq); (b) KCl(aq); (c) $MgCl_2$(aq); (d) $CaCl_2$(aq); (e) Na_2SO_4(aq); (f) $NaHCO_2$(aq).

Table 8
Parameters in the solubility model.[a]

$A_0 = -1.23$	$A_1 = -8.85$	$A_2 = 17.91$	
$k_{12,0} = 0.1070$	$k_{12,1} = -0.2447$	$k_{21,0} = 0.2606$	$k_{21,1} = -0.0284$
$\delta_{1,0} = 1.0310$	$\delta_{1,1} = -0.2489$	$\delta_{2,0} = 0.7149$	$\delta_{2,1} = 0.2475$
$\delta_{3,0} = 1.9327$	$\delta_{3,1} = 0.1267$	$\delta_{4,0} = 2.0390$	$\delta_{4,1} = -0.2093$
$\delta_{5,0} = 0.1688$	$\delta_{5,1} = -0.4291$	$\delta_{6,0} = 0.0899$	$\delta_{6,1} = -0.7102$

[a] Subscript i in δ_{ij} denotes the ion: 1 = Na^+, 2 = K^+, 3 = Mg^{2+}, 4 = Ca^{2+}, 5 = SO_4^{2-}, 6 = HCO_3^-.

or equilibrium) at temperatures from the triple point of pure water T_w up to the upper critical endpoint temperature $T_{UCEP} = 304.63$ K [25]. The IFT γ along an isotherm at $T_w \leq T < T_{UCEP}$ is therefore divided into two branches according to whether the pressure is below or above the three–phase coexistence pressure $p_3(T)$. At pressures below p_3, one has vapor–liquid coexistence whereas, above p_3, liquid–liquid equilibrium exists. At $p = p_3$, three phases and three IFTs coexist: CO_2–rich vapor, CO_2–rich liquid and H_2O–rich liquid. The IFT between the CO_2–rich vapor and the CO_2–rich liquid is very small, vanishing as $T \to T_{UCEP}$, and is not considered explicitly in this work. At temperatures above T_{UCEP}, a gaseous or super–critical phase, usually rich in CO_2, coexists with a H_2O–rich liquid phase.

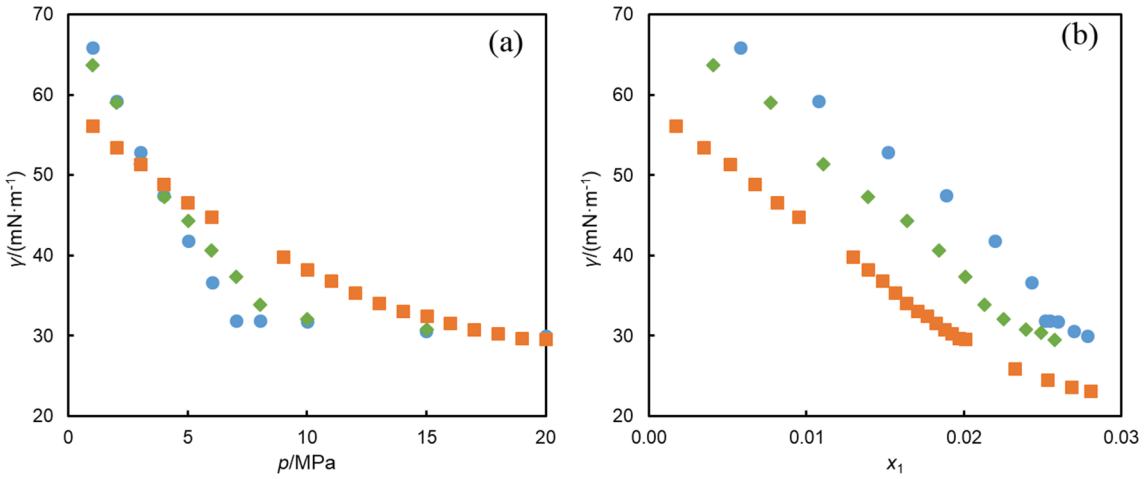


Fig. 4. Interfacial tension γ of the ($CO_2 + H_2O$) system as a function of (a) pressure p and (b) mole fraction x_1 of CO_2 dissolved in the aqueous phase: ●, $T = 297.8$ K; ◆, $T = 312.9$ K; ■, $T = 374.3$ K [111,112].

The relative difficulty of finding a simple but accurate and wide–ranging empirical representation of the IFT of the ($CO_2 + H_2O$) binary system in terms of temperature and pressure is illustrated in Fig. 4 (a). The subcritical isotherms exhibit essentially bilinear behavior with a small discontinuity at $p = p_3$, a large slope in the vapor–liquid region and a smaller one at higher pressures in the liquid–liquid region. At a temperature slightly above T_{UCEP} (exemplified by the data at $T = 312.9$ K) the isotherm is continuous but still exhibits a rapid change of slope dividing it into two nearly–linear regions. On the other hand, isotherms at temperatures well above T_{UCEP} become smooth and continuous. These observations suggest that a correlation explicit in pressure may not be easily achieved. At a fundamental level, the IFT is controlled by the surface excess concentration of CO_2 at the interface, which increases rapidly with the density of the CO_2–rich phase. As a proxy for the surface excess, we propose the mole fraction x_1 of CO_2 dissolved in the aqueous phase which, although different in magnitude, varies in a similar way. Fig. 4(b) shows the same IFT data plotted against x_1 and one can see that behavior is greatly simplified and all isotherms approach the surface tension of pure water γ_w as $x_1 \to 0$. Note that, at $T < T_{UCEP}$, the isotherms are still discontinuous in value at the three–phase pressure; therefore a piecewise representation of the data is required.

In developing the correlation, we define a dimensionless IFT difference

$$\Delta\tilde{\gamma} = (\gamma_w - \gamma)/(\mathrm{mN{\cdot}m^{-1}}) \tag{30}$$

where the water surface tension γ_w was calculated from the IAPWS correlation [113], re–written here in terms of the reduced temperature τ:

$$\gamma_w/(\mathrm{mN{\cdot}m^{-1}}) = 235.8\{1-(1+\tau)(T_{UCEP}/T_c)\}^{1.256}[1-0.625\{1-(1+\tau)(T_{UCEP}/T_c)\}] \tag{31}$$

where $T_c = 647.096$ K is the critical temperature of water. We also define the CO_2 mole fractions $x_3(\tau)$ on the three–phase line,

$$x_3(\tau) = x_1(\tau, p_3) \tag{32}$$

where p_3 is the three–phase pressure and $x_1(\tau, p_3)$ is the CO_2 solubility evaluated from new model for the desired phase. The three phase pressure is conveniently represented by the correlation of Wendland et al. [25], again re–written in terms of reduced temperature:

$$\ln(p_3/\mathrm{MPa}) = 3.99263 - 1335.97[(1+\tau)(T_{UCEP}\ /\ \mathrm{K})]^{-1} + 0.007865[(1+\tau)(T_{UCEP}\ /\ \mathrm{K})] \tag{33}$$

Considering first the region at temperatures well above T_{UCEP}

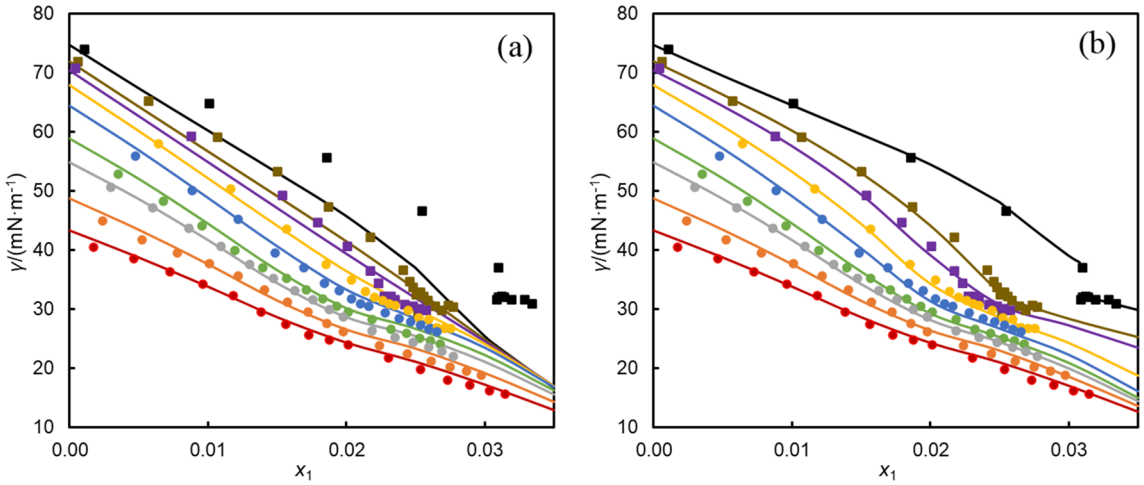


Fig. 5. Interfacial tension γ as a function of CO_2 mole fraction x_1 in the aqueous phase along selected isotherms in comparison with the model: (a) restricted correlation neglecting, and; (b) full correlation. Experimental data: ●, Li et al. [114]; ■, Hebach et al. [115]. Lines represent the correlation and colors denote temperature: black, $T = 279$ K; brown, $T = 298$ K; purple, $T = 308$ K; yellow, $T = 323$ K; blue, $T = 343$ K; green, $T = 373$ K; grey, $T = 393$ K; orange, $T = 423$ K; red, $T = 448$ K. (For interpretation of the references to colour in this figure legend, the reader is referred to the web version of this article.)

(practically, $T \gtrsim 323$ K), the following equation was found to provide a good description of $\Delta\widetilde{\gamma}$:

$$\Delta\widetilde{\gamma}_1(\tau, x_1) = \left[b_1 + b_2\tau\tanh\left(b_3\tau + b_4x_1 + b_5x_1^4\right)\right]x_1 \quad (34)$$

The functional form of Eq. (34) was derived in part by use of a symbolic regression tool (Eureqa version 1.24, Nutonian, Inc.). Fig. 5(a) compares selected data along several isotherms with a preliminary analysis in which the parameters of Eq. (34) were fitted to data at $T \geq 323.15$ K. It demonstrates rather good agreement at those temperatures but substantial differences at lower temperatures. Below the upper critical end–point temperature, the isotherms split into two branches and must be parameterized by separate functions that join to become continuous at $T = T_{UCEP}$. For temperatures slightly above T_{UCEP} the isotherms still deviate from Eq. (34) indicating that the full correlation requires, in addition to the term $\Delta\gamma_1$, functions that correct both the sub–critical and near–critical regions. Therefore, in the full correlation, the IFT is modelled in two domains with the following general forms:

$$\Delta\widetilde{\gamma}(\tau, x_1 \leqslant x_3) = \Delta\widetilde{\gamma}_1(\tau, x_1) + \Delta\widetilde{\gamma}_2(\tau, x_1) \quad (35)$$

$$\Delta\widetilde{\gamma}(\tau, x_1 > x_3) = \Delta\widetilde{\gamma}_1(\tau, x_1) + \Delta\widetilde{\gamma}_3(\tau) + \Delta\widetilde{\gamma}_4(\tau, x) \quad (36)$$

Here, $\Delta\widetilde{\gamma}_2$ primarily corrects the behavior in the gas–liquid region ($\tau \leq 0, x_1 \leq x_3$) and decays rapidly in the region $\tau > 0$. In Eq. (36), the term $\Delta\widetilde{\gamma}_3$ represents the change in the IFT occurring at the three phase pressure (zero for $\tau > 0$), while $\Delta\widetilde{\gamma}_4$ corrects the behavior in the liquid–liquid region ($\tau > 0, x_1 > x_3$) and decays rapidly in the region $\tau > 0$. Based on the analysis of the behavior observed in Fig. 4, the following functional forms were selected for $\Delta\widetilde{\gamma}_2$ and $\Delta\widetilde{\gamma}_4$:

$$\Delta\widetilde{\gamma}_2 = \left[b_6\left\{1 + (b_7 + b_8\tau)x_1^2\right\}x_1\right]F(\tau) \quad (37)$$

$$\Delta\widetilde{\gamma}_4 = b_6\left[\left\{1 + (b_7 + b_8\tau)x_3^2\right\}x_3 + (b_9 + b_{10}\tau)(x_1 - x_3)\right]F(\tau) \quad (38)$$

where F(τ) is a damping function defined by

$$\left.\begin{array}{c} F(\tau \leqslant 0) = 1 \\ F(\tau > 0) = \exp(-b_{12}\tau) \end{array}\right\} \quad (39)$$

Eqs. (37) and (38) have the property that $\Delta\widetilde{\gamma}_2(\tau, x_3) = \Delta\widetilde{\gamma}_4(\tau, x_3)$ which ensures that the correlation is continuous in value when $\tau \geq 0$. At sub–critical temperatures, the change in the IFT occurring upon crossing the three–phase line, represented by $\Delta\widetilde{\gamma}_3$, is a manifestation of the IFT between water–saturated CO_2–rich vapor and water–saturate CO_2–rich liquid and is expected to follow trend similar to the surface tension of pure CO_2. Therefore, we adopted a one–parameter representation as follows:

Table 9
Literature data for IFT of the (CO_2 + H_2O) system.[1]

Source	T/K	p/MPa	N	Δ_{AAD}	Note
Hebach et al. [115]	278–308	0.1–20	84/85	0.6	2
Georgiadis et al. [111]	297–375	1–60	76/80	0.5	2
Li et al. [114]	323–448	2–50	96/96	0.6	2, 3
Pereira et al. [117]	298–343	0.3–69	77/78	0.7	2
Khosharay et al. [118]	284–313	1–20	27/30	1.4	4
Chiquet et al. [120]	308–383	5–45	0/43	1.5	2
Liu et al. [121]	301–352	2.9–12	0/209	1.3	4
Bachu et al. [122]	309–399	2–27	0/42	6.2	5
Chun et al. [123]	298–345	0.1–19	0/125	5.2	6
Jho et al. [124]	298–319	0.1–5.8	0/62	0.4	6
Bikkina et al. [125]	298–314	1.5–21	0/36	4.4	4
Liu et al. [126]	299–346	1.2–33	0/36	1.8	5

[2] Pendant–drop method, $\Delta\rho$ recalculated in this work according to the method of Chow et al.[112].
[3] Extrapolated to zero molality from CO_2–brine data.
[4] Pendant–drop method, $\Delta\rho$ calculated by original authors.
[5] Pendant–drop method, $\Delta\rho$ measured by original authors.
[6] Capillary–rise method.
[1] N is the number of aqueous phase data points used/reported.

$$\Delta\widetilde{\gamma}_3(\tau \leqslant 0) = b_{11}|\tau|^{1.25} \quad (40)$$

Finally, for saline systems, the water surface tension is replaced by the surface tension γ_b of the brine, which was correlated in the form proposed by Li et al. [116]:

$$(\gamma_b - \gamma_w)/(\mathrm{mN{\cdot}m^{-1}}) = [b_{13} + b_{14}\tau](m^+ / m^\circ) \quad (41)$$

where $m^\circ = 1$ mol·kg^{-1}, and m^+ is the sum of the charge–weighted cation molalities:

$$m^+ = \sum_{\text{cations}} z_i m_i \quad (42)$$

Here, z_i is the charge number, m_i is the molality of cation i. The key feature of this equation, convincingly demonstrated in [116], is that (γ_b – γ_w) is proportional to m^+ with a coefficient that is a weak function of temperature. For all the electrolytes considered in this work, $\gamma_b \geq \gamma_w$.

3.2. Experimental data

A substantial body of experimental data, summarized in Table 9, have been reported in the literature. Unfortunately, the agreement between different sources is not always good and the reasons for this have been discussed in the literature [111]. To build the present correlation for the (CO_2 + H_2O) binary system, we relied upon a selected set of primary data [111,114,115,117,118], all of which were measured by the pendant drop method. One of the issues in this experimental method is that the density difference $\Delta\rho$ between the saturated phases is a required input. The density difference between the aqueous and non–aqueous phases is generally close to that between pure water and carbon dioxide at the same conditions of temperature and pressure. However, the dissolution of CO_2 makes a small but significant difference to the density of the aqueous phase which has an important influence on the density difference at low temperature and high pressures where $\Delta\rho$ is small. This effect can be modelled accurately using the new solubility model developed in this work together with the density of pure water from the IAPWS–95 equation of state [75] and the partial molar volume of CO_2 from the correlation of Sedlbauer et al. [77]. The effect of H_2O in the non–aqueous phase is much less important, being significant only at high temperatures and low pressures [112]. In our analysis, we have recalculated the density differences between the phases and applied our values to correct the data of Hebach et al. [115], Georgiadis et al. [111] and Pereira et al. [117]. The data of Li et al. [114] for the (CO_2 + H_2O) system were obtained by extrapolating an extensive set of (brine + CO_2) to the limit of zero salt molality. In this work, we first applied corrections to bring the density differences into agreement with the present model and then recalculated the extrapolations. All recalculated data are available in the Supplementary Information.

Table 10 details the literature data considered for (CO_2 + brine) systems and includes both the salt(s) and the range of molalitity studied. In parameterizing the model, we relied upon the extensive data reported by Li et al. [114,116] and Li [119]; the other literature sources were used for comparison.

3.3. (CO_2 + H_2O) binary system

The model was initially fitted separately to in regions where the CO_2–rich phase is gas, liquid and supercritical. A final fit to all data together was then performed and the resulting parameters are given in Table 11. The overall AARD for the 363 primary data points was 1.8% and the RMSD is 0.8 mN·m^{-1}. Fig. 5(b) and 6 compares these data with the model and one can observe good agreement in all regions of the phase diagram with all but a few data points falling within ± 2 mN·m^{-1} of the fit. Fig. 5(b) shows the isotherm at $T = 279$ K which is split into vapor–liquid and liquid–liquid branches with a jump in the IFT when crossing the three-phase line. Fig. 6(a) also shows the three-phase region

Table 10
Literature data for IFT of (CO_2 + brine) systems.[1.]

Source	Salts	m/(mol·kg^{-1})	T/K	p/MPa	N	Δ_{AAD}
Chalbaud [5]	NaCl	0.085–2.75	300–373	4–25	72	3.9
Pereira [127]	NaCl	0.98–1.98	298–423	3–70	30	0.7
Aggelopoulo [128]	$CaCl_2$	0.045–2.7	300–373	4.9–25	67	1.9
Aggelopoulo [129]	NaCl + $CaCl_2$	0.045–1.5	300–373	5–26	63	1.8
Li et al. [114]	NaCl + KCl	0.98–4.95	298–423	2–50	304	0.6
Li et al. [116]	$CaCl_2$, $MgCl_2$	0.5–5	343–423	2–50	208	1.0
	Na_2SO_4	0.98–1.96	353–373	2–50	24	0.7
	$NaHCO_3$	0.98	343–423	2–50	62	0.6
Li [119]	NaCl	1.0	473	2–40	7	0.5
	Multi–component	0.4 – 2.3	343–393	2–40	21	0.7
Liu [121]	NaCl	0.2–1.8	300–354	2–12	114	1.4
Mutailipu [130]	NaCl + KCl	0.98–4.95	298–423	2–15	120	1.3

Table 11
Parameters of the IFT model.

b_1	b_2	b_3	b_4	b_5	b_6	b_7
1546.4	–1439.2	4.0159	–63.118	4,414,244	–430.7	–2250.9
b_8	b_9	b_{10}	b_{11}	b_{12}	b_{13}	b_{14}
–27889	–966.9	3169	124.5	14	1.608	1.072

in γ-T coordinates. Referring to Table 9, the secondary data of Chiquet et al. [120], Liu et al. [121], Jho et al. [124] and Liu et al. [126] all show good agreement with the model, while those of Bachu et al. [122], Chun et al. [123] and Bikkina et al. [125] deviate substantially.

3.4. (CO_2 + brine) system

For the brine systems, only an additional two parameters were required, describing the increase in the surface tension of the brine as a function of m^+ and τ. The parameters are given in Table 11 and the fit to the 626 primary data points show an AARD of 1.7% and a standard deviation of 0.8 mN·m^{-1}. Fig. 7 compares the brine data with the model as functions of both pressure and charge–weighted cation molality. As with the (CO_2 + H_2O) binary system, all but a few points fall within ± 2 mN·m^{-1}. There appears to be no systematic dependence of the deviation on molality. Although there is no significant overall bias, the deviations are predominantly negative at low pressures and positive at high pressures.

4. Discussion and conclusions

By considering the IFT in the CO_2–H_2O binary system as a function of temperature and CO_2 mole fraction, a comparatively simple, wide–ranging and continuous correlation can been constructed. This is extended to CO_2–brine systems with a further two parameters only. The overall model is able to predict the IFT generally within ± 2 mN·m^{-1}, which is probably about the best that can be expected based on the available experimental data. Specifically, for the IFT of the CO_2-H_2O binary system, the overall RMSD of the experimental data from our model is 0.65 mN·m^{-1} while the AARD is 1.8%; similar figures apply to the CO_2-brine systems. The present model is more comprehensive than previous approaches in terms of brine chemistry and/or temperature and pressures ranges. It is straight-forward to implement, although it does require the mutual solubility model to be invoked at every state point. As a simple empirical correlation, the IFT model is much faster to compute than theoretical approaches such as molecular dynamics or density gradient theory.

To facilitate development of the IFT model, a revised and improved model for the mutual solubility of CO_2–brine systems has also been developed. This is an improvement over previous models, such as those of Spycher and Pruess [42] and Duan [40]. The RMSD of CO_2 mole fraction in the aqueous phase is 0.0003 and the AARD is 5.5% while, in the non-aqueous phase, the RMSD of H_2O mole fraction is 0.0035 and the corresponding AARD is 8.7%. The mutual solubility model is based on the well-established γ-φ approach with the PR-EoS being used for the non-aqueous phase and a simple activity-coefficient model being used

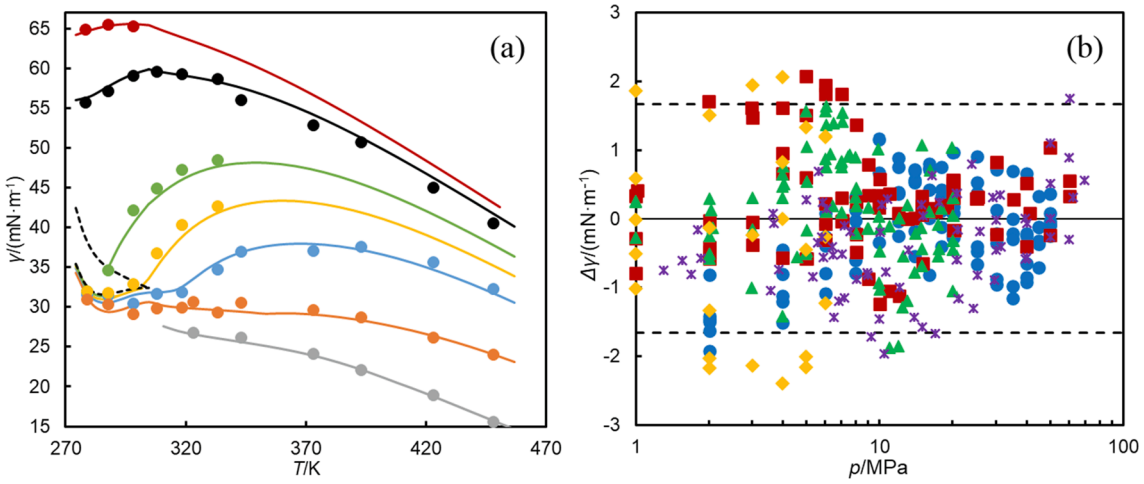


Fig. 6. (a) Interfacial tension γ of (CO_2 + H_2O) as a function of temperature T along isobars comparing interpolated experimental data (●) with the new model (solid curves): red, p = 1 MPa; black, p = 2 MPa; green, p = 5 MPa; yellow, p = 7 MPs; blue, p = 10 MPa; orange, p = 20 MPa; grey, p = 50 MPs. Dashed curves show the predicted IFTs on the three–phase line. (b) deviations $\Delta\gamma$ of experimental interfacial tensions of (CO_2 + H_2O) from the new model as a function of pressure p: ■, Georgiadis et al. [111]; ●, Li et al. [114].; *, Pereira et al. [117]; △, Hebach et al. [115]; ◆, Khosharay et al. [118]. Dashed lines show the 95% confidence interval of the model. (For interpretation of the references to colour in this figure legend, the reader is referred to the web version of this article.)

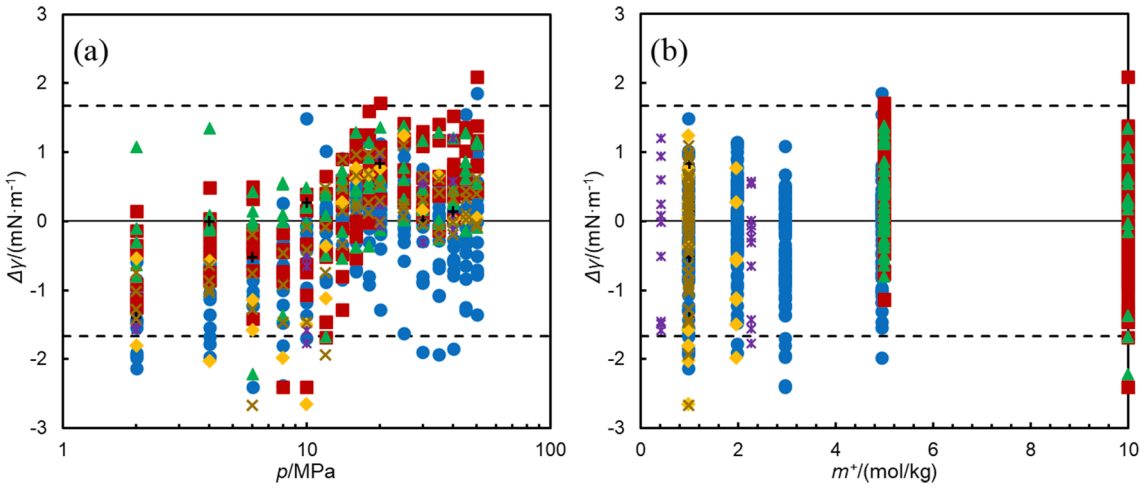


Fig. 7. Deviations $\Delta\gamma$ of experimental interfacial tensions of (CO_2 + brine) from the new model as a function of (a) pressure p and (b) charge–weighted cation molality m^+. Experimental data: ●, NaCl/KCl mixed brine [114], ■, $CaCl_2$(aq) [116], △, $MgCl_2$(aq) [116], ◆, Na_2SO_4(aq) [116], ×, $NaHCO_3$(aq) [116], +, NaCl (aq) [119], *, multi–component brine [119]. Dashed lines show the 95% confidence interval of the model.

for the aqueous phase. It is parameterized for the same brine chemistries as the IFT model. While the model is simple, a possible disadvantage is that an iterative solution is required making the approach marginally slower but more wide-ranging than the non-iterative scheme of Spycher et al. [15]. In terms of complexity, and hence computational efficiency, the present approach is comparable to other models utilising simple equations of state such as those of Duan et al. [40], Spycher and Pruess [42], or Parkhurst and Appelo, 2013 [52–54].

The current models are not recommended for extrapolation to temperatures above about 473 K or to pressures above 70 MPa for IFT and 100 MPa for mutual solubility.

On the basis of results, the following conclusions can be drawn:

1. Use of temperature and CO_2 mole fraction in the aqueous phase allows a smooth and continuous correlation to be built for the IFT of the CO_2–water system.
2. A simple term, linear in both temperature and the sum of the charge–weighted cation molalities, adequately describes the IFT increment due to dissolved salts up to a salt molality of 5 mol·kg^{-1}.
3. The new model for mutual solubility gives excellent results and accounts for new data that were not available in the construction of earlier models. The use of salting–out parameters that distinguish between cations of the same charge is especially helpful in this regard.
4. The two models cover in full the ranges of temperature and pressure relevant to GCS. They also apply to a wide range of brine chemistries through consideration of seven important ions. The carbonate ion is not specifically considered but, in the presence of CO_2, equilibrium favors bicarbonate and so this should not be a limitation. Other minor ions are not expected to influence the properties studied significantly are these could sensibly be lumped with one of the ions in the model having the same charge. Impurities that might be present in the CO_2 stream are not considered in this work.

CRediT authorship contribution statement

Meiheriayi Mutailipu: Writing – original draft, Software, Investigation, Formal analysis. **Yongchen Song:** Writing – review & editing, Validation, Supervision, Funding acquisition. **Qiang Yao:** Writing – review & editing, Supervision, Funding acquisition. **Yu Liu:** Writing – review & editing, Validation, Supervision. **J.P. Martin Trusler:** .

Declaration of Competing Interest

The authors declare that they have no known competing financial interests or personal relationships that could have appeared to influence the work reported in this paper.

Data availability

Data available in Supplementary Material

Acknowledgments

This work was supported by the funding from Central guide for the development of local technology specific fund (grant number ZYYD2022C16), Special Project for key Research and Development Program of Xinjiang Autonomous Region (grant number 2022B01033–2), Xinjiang Autonomous Region Innovation Environment (talents, base) construction special project–youth fund for natural science (grant number 2021D01C089).

Appendix A

Equation of State.

The PR-EoS is given by

$$p = \frac{RT}{V_m - b} - \frac{a}{V_m(V_m + b) + b(V_m - b)} \tag{A–1}$$

where p is pressure, T is temperature, R is the universal gas constant and V_m is molar volume. For a pure substance,

$$a = 0.45724\frac{(RT_c)^2}{p_c}\alpha(T), \tag{A–2}$$

$$b = 0.07780\frac{(RT_c)}{p_c}, \tag{A–3}$$

$$\alpha(T) = \left[1 + (0.7464 + 1.54226\omega - 0.26992\omega)\left(1 - \sqrt{T/T_c}\right)\right]^2 \tag{A–4}$$

where T_c and p_c are the critical temperatures and pressures, respectively, and ω is the acentric factor. To solve the equation of state for the compressibility factor $Z = pV_m/RT$, equation (A–1) can be put into a standard cubic form,

$$Z^3 - (1 - B)Z^2 + (A - 3B^2 - 2B)Z - (AB - B^2 - B^3) = 0, \tag{A–5}$$

and solved analytically. Here A and B are dimensionless parameters given by $A = ap\ /\ (RT)^2$ and $B = bp\ /\ (RT)$. For mixtures, the parameters a and b are obtained from the standard one–fluid mixing rules as follows:

$$a = \sum_i \sum_j y_i y_j a_{ij} \tag{A–6}$$

$$b = \sum_i y_i b_i \tag{A–7}$$

Here, y_i denotes mole fraction of component i, a_{ii} and b_i are the a and b parameters for pure component i and a combining rule is used to obtain the unlike term a_{ij} as discussed in the main text.

Appendix B. Supplementary material

Supplementary data to this article can be found online at https://doi.org/10.1016/j.fuel.2023.129712.

References

[1] Rogelj J, den Elzen M, Höhne N, Fransen T, Fekete H, Winkler H, et al. Paris Agreement climate proposals need a boost to keep warming well below 2 °C. Natur 2016;534(7609):631–9.

[2] Ipcc. Climate Change 2021: The Physical Science Basis. Contribution of Working Group I to the Sixth Assessment Report of the Intergovernmental Panel on Climate Change. Cambridge, United Kingdom and New York, NY, USA: Cambridge University Press; 2021.

[3] Peridas G, Mordick SB. The role of carbon capture and storage in the race to carbon neutrality. Electr J 2021;34(7):106996.

[4] Al-Bazali TM, Zhang J , Chenevert M E, Sharma M M. Measurement of the Sealing Capacity of Shale Caprocks. *Special Report on Carbon Dioxide Capture and Storage IPCC.* SPE Annual Technical Conference and Exhibition, Houston, Texas 2005: 431.

[5] Chalbaud C, Robin M, Lombard J, Martin F, Egermann P, Bertin H. Interfacial tension measurements and wettability evaluation for geological CO_2 storage. Adv Water Resour 2009;32(1):98–109.

[6] Irfan MF, Bisson TM, Bobicki E, Arguelles-Vivas F, Xu Z, Liu Q, et al. CO_2 storage in saline aquifers by dissolution and residual trapping under supercritical conditions: An experimental investigation. Colloids Surf A Physicochem Eng Asp 2018;548:37–45.

[7] Rosenbauer RJ, Thomas B. Carbon dioxide (CO_2) sequestration in deep saline aquifers and formations. Developments and Innovation in Carbon Dioxide (CO_2) Capture and Storage Technology. Woodhead Publishing 2010:57–103.

[8] Coan CR. King A D Solubility of water in compressed carbon dioxide, nitrous oxide, and ethane: Evidence for hydration of carbon dioxide and nitrous oxide in the gas phase. J Am Chem Soc 1971;93:1857–62.

[9] Carroll JJ. Mather A E The system carbon dioxide-water and the Krichevsky-Kasarnovsky equation. J Solution Chem 1992;21(7):607–21.

[10] King MBMA, Kim JD, Bott TR. The mutual solubilities of water with supercritical and liquid carbon dioxides. J Supercrit Fluids 1992;5(4):296–302.

[11] Duan ZMN, Weare JH. An equation of state for the CH_4-CO_2-H_2O system: II. Mixtures from 50. Geochim Cosmochim Acta 1992;56:2619–31. to 1000°C and 0 to 1000 bars.

[12] Shyu G-S, Hanif NSM, Hall KR, Eubank PT. Carbon dioxide-water phase equilibria results from the Wong-San dler combining rules. Fluid Phase Equilib 1997;130: 73–85.

[13] Bamberger A, Sieder G, Maurer G. High-pressure (vapor+liquid) equilibrium in binary mixtures of (carbon dioxide+water or acetic acid) at temperatures from 313 to 353 K. J Supercrit Fluids 2000;17(2):97–110.

[14] Jörn K, Horstmann S, Fischer K, Gmehling J. Experimental Determination and Prediction of Gas Solubility Data for CO_2 + H_2O Mixtures Containing NaCl or KCl at Temperatures between 313 and 393 K and Pressures up to 10 MPa. Ind Eng Chem Res 2002;41(17):4393–8.

[15] Spycher N, Pruess K, Ennis-King J. CO_2-H_2O mixtures in the geological sequestration of CO_2. I. Assessment and calculation of mutual solubilities from 12 to 100°C and up to 600 bar. GeCoA 2003;67(16):3015–31.

[16] Diamond LWANN. Solubility of CO_2 in water from −1.5 to 100 °C and from 0.1 to 100 MPa: evaluation of literature data and thermodynamic modelling. Fluid Phase Equilib 2003;208(1):265–90.

[17] Chapoy A, Mohammadi AH, Chareton A, Tohidi B, Richon D. Measurement and Modeling of Gas Solubility and Literature Review of the Properties for the Carbon Dioxide−Water System. Ind Eng Chem Res 2004;43(7):1794–802.

[18] Valtz A, Chapoy A, Coquelet C, Paricaud P, Richon D. Vapour–liquid equilibria in the carbon dioxide–water system, measurement and modelling from 278.2 to 318.2K. Fluid Phase Equilib 2004;226:333–44.

[19] Siqueira Campos CEP, Villardi HGDA, Pessoa FLP, Uller AMC. Solubility of Carbon Dioxide in Water and Hexadecane: Experimental Measurement and Thermodynamic Modeling. J Chem Eng Data 2009;54(10):2881–6.

[20] Tabasinejad F, Moore RG, Mehta SA, Fraassen KCV, Barzin Y, Rushing JA, et al. Water Solubility in Supercritical Methane, Nitrogen, and Carbon Dioxide: Measurement and Modeling from 422 to 483 K and Pressures from 3.6 to 134 MPa. Ind Eng Chem Res 2011;50:4029–41.

[21] Hou S-X, Maitland GC, Trusler JPM. Measurement and modeling of the phase behavior of the (carbon dioxide+water) mixture at temperatures from 298.15K to 448.15K. J Supercrit Fluids 2013;73:87–96.

[22] Jiang CYW, JF, Sun ZJ, Pan QM. Solubility of water in supercritical CO_2. Huaxue Gongcheng Xi'an 2014;42(7):42-7.

[23] Hemmati-Sarapardeh A, Amar MN, Soltanian MR, Dai Z, Zhang X. Modeling CO_2 Solubility in Water at High Pressure and Temperature Conditions. Energy Fuel 2020;34:4761–76.

[24] Scott RL, van Konynenburg PH. Critical lines and phase equilibria in binary van der Waals mixtures. Philos Trans Royal Soc 1980;298(1442):495–540.

[25] Wendland M, Hasse H, Maurer G. Experimental Pressure-Temperature Data on Three- and Four-Phase Equilibria of Fluid, Hydrate, and Ice Phases in the System Carbon Dioxide−Water. J Chem Eng Data 1999;44(5):901–6.

[26] Crovetto R. Evaluation of Solubility Data of the System CO_2-H_2O from 273 K to the Critical Point of Water. J Phys Chem Ref Data 1991;20(3):575–89.

[27] Carroll JJSJD, Mather AE. The Solubility of Carbon Dioxide in Water at Low Pressure. J Phys Chem Ref Data 1991;20(6):1201–9.

[28] Fernandez-Prini R, Alvarez JL, Harvey AH. Henry's constants and vapor-liquid distribution constants for gaseous solutes in H_2O and D_2O at high temperatures. J Phys Chem Ref Data 2003;32(2):903–16.

[29] Paricaud P, Galindo A, Jackson G. Recent advances in the use of the SAFT approach in describing electrolytes, interfaces, liquid crystals and polymers. Fluid Phase Equilib 2002;194–197:87–96.

[30] Khoshraftar Z, Ghaemi A. Prediction of CO_2 solubility in water at high pressure and temperature via deep learning and response surface methodology. Case Stud Therm Eng 2023;7:100338.

[31] Wong DSH, Sandler SI. A theoretically correct mixing rule for cubic equations of state. AIChE 1992;38(5):671–80.

[32] Kontogeorgis GM, Michelsen ML, Folas GK, Derawi S, von Solms N, Stenby EH. Ten years with the CPA (Cubic-Plus-Association) equation of state. Part 1. Pure compounds and self-associating systems. Ind Eng Chem Res 2006;45(14): 4855–68.

[33] Kontogeorgis GM, Michelsen ML, Folas GK, Derawi S, von Solms N, Stenby EH. Ten Years with the CPA (Cubic-Plus-Association) Equation of State. Part 2. Cross-Associating and Multicomponent Systems. Ind Eng Chem Res 2006;45(14): 4869–78.

[34] Míguez JM, dos Ramos MC, Piñeiro MM, Blas FJ. An Examination of the Ternary Methane + Carbon Dioxide + Water Phase Diagram using the SAFT-VR Approach. J Phys Chem B 2011;115(31):9604–17.

[35] Pitzer KS. Thermodynamics of Electrolytes. I. Theoretical Basis and General Equations. J Phys Chem 1973;77(2):268–77.
[36] Pitzer KS. Thermodynamics of Electrolytes.V. Effects of higher-order electrostatic terms. J Solution Chem 1975;4(3):249–65.
[37] Pitzer KS, Mayorga G. Thermodynamics of Electrolytes. II. Activity and Osmotic Coefficients for Strong Electrolytes with One or Both Ions Univalent. J Phys Chem 1973;77(19):2300–8.
[38] Pitzer KS. Activity coefficients in electrolyte solutions. Boca Raton: CRC Press; 1991.
[39] Duan Z, Sun R. An improved model calculating CO_2 solubility in pure water and aqueous NaCl solutions from 273 to 533 K and from 0 to 2000 bar. ChGeo 2003;193(3–4):257–71.
[40] Duan Z, Sun R, Zhu C, Chou IM. An improved model for the calculation of CO_2 solubility in aqueous solutions containing Na^+, K^+, Ca^{2+}, Mg^{2+}, Cl^-, and SO_4^{2-}. Mar Chem 2006;98(2–4):131–9.
[41] Spycher N, Pruess K. CO_2-H_2O mixtures in the geological sequestration of CO_2. II. Partitioning in chloride brines at 12–100°C and up to 600 bar. GeCoA 2005;69(13):3309–20.
[42] Spycher N, Pruess K. A Phase-Partitioning Model for CO_2–Brine Mixtures at Elevated Temperatures and Pressures: Application to CO_2-Enhanced Geothermal Systems. TPM 2010;82(1):173–96.
[43] Bowers TS, Helgeson HC. Calculation of the thermo dynamic and geochemical consequences of nonideal mixing in the system H_2O-CO_2-NaCl on phase relations in geologic systems: Equation of state for $_H2O$-C_O2-NaCl fluids at high pressures and temperatures. Geochim Cosmochim Acta 1983;47:1247–75.
[44] Rumpf B, Nicolaisen H, Öcal C, Maurer G. Solubility of carbon dioxide in aqueous solutions of sodium chloride: Experimental results and correlation. J Solution Chem 1994;23(3):431–48.
[45] Duan Z, Møller N, Weare H. Equation of state for the NaCl-H_2O-CO_2 system: Prediction of phase equilibria and volu metric properties. Geochim Cosmochim Acta 1995;59:2869–82.
[46] Bando S, Takemura F, Nishio M, Hihara E, Akai M. Solubility of CO_2 in Aqueous Solutions of NaCl at (30 to 60) °C and (10 to 20) MPa. J Chem Eng Data 2003;48(3):576–9.
[47] Bermejo MD, Martín A, Florusse LJ, Peters CJ, Cocero MJ. The influence of Na_2SO_4 on the CO_2 solubility in water at high pressure. Fluid Phase Equilib 2005;238(2):220–8.
[48] Yan YZ, Chen CC. Thermodynamic modeling of CO_2 solubility in aqueous solutions of NaCl and Na_2SO_4. J Supercrit Fluids 2010;55(2):623–34.
[49] Springer RDWZ, Anderko A, Wang P, Felmy AR. A thermodynamic model for predicting mineral reactivity in supercritical carbon dioxide: I. Phase behavior of carbon dioxide–water–chloride salt systems across the H_2O-rich to the CO_2-rich regions. ChGeo 2012;322(323):151–71.
[50] Hou S-X, Maitland GC, Trusler JPM. Phase equilibria of (CO_2+H_2O+NaCl) and (CO_2+H_2O+KCl): Measurements and modeling. J Supercrit Fluids 2013;78:78–88.
[51] Bastami A, Allahgholi M, Pourafshary P. Experimental and modelling study of the solubility of CO_2 in various $CaCl_2$ solutions at different temperatures and pressures. Pet Sci 2014;11(4):569–77.
[52] Parkhurst DL, Appelo C. Description of input and examples for PHREEQC version 3—a computer program for speciation, batch-reaction, one-dimensional transport, and inverse geochemical calculations. US geological survey techniques methods 2013;6(A43):497.
[53] Appelo CAJ, Parkhurst DL, Post VEA. Equations for calculating hydrogeochemical reactions of minerals and gases such as CO_2 at high pressures and temperatures. GeCoA 2014;125:49–67.
[54] Appelo CAJ. Principles, caveats and improvements in databases for calculating hydrogeochemical reactions in saline waters from 0 to 200 °C and 1 to 1000 atm. Appl Geochem 2015;55:62–71.
[55] Zhao H, Dilmore RM, Lvov SN. Experimental studies and modeling of CO_2 solubility in high temperature aqueous $CaCl_2$, $MgCl_2$, Na_2SO_4, and KCl solutions. AIChE 2015;61(7):2286–97.
[56] dos Santos PF, André L, Ducousso M, Lassin A, Contamine F, Lach A, et al. An improved model for CO_2 solubility in aqueous Na^+–Cl^-–SO_4^{2-} systems up to 473.15 K and 40 MPa. ChGeo 2021;582:120443.
[57] Sun X, Wang Z, Li H, He H, Sun B. A simple model for the prediction of mutual solubility in CO_2-brine system at geological conditions. Desalination 2021;504:114972.
[58] Ratnakar RR, Chaubey V, Dindoruk B. A novel computational strategy to estimate CO_2 solubility in brine solutions for CCUS applications. ApEn 2023;342:121134.
[59] Ratnakar RR, Venkatraman A, Kalra A, Dindoruk B. On the prediction of gas solubility in brine solutions with single or mixed salts: Applications to gas injection and CO_2 capture/sequestration. J Nat Gas Sci Eng 2020;81:103450.
[60] Westacott RE, Rocha S, Johnston KP, Rossky PJ. Molecular Structure of the Water - Supercritical Carbon Dioxid Interface. J Phys Chem 2001;105(48):12092–104.
[61] Kuznetsova T, Kvamme B. Thermodynamic properties and surface tension of model water-carbon dioxide systems. PCCP 2002;4(6):937–41.
[62] Nielsen LC, Bourg IC, Sposito G. Predicting CO_2-water interfacial tension under pressure and temperature conditions of geologic CO_2 storage. GeCoA 2012;81:28–38.
[63] Georgiadis A, Llovell F, Bismarck A, Blas FJ, Galindo A, Maitland GC, et al. Interfacial tension measurements and modelling of (carbon dioxide plus n-alkane) and (carbon dioxide plus water) binary mixtures at elevated pressures and temperatures. J Supercrit Fluids 2010;55(2):743–54.
[64] Kashefi K. Measurement and modelling of interfacial tension and viscosity of reservoir fluids. Heriot-Watt University; 2012.
[65] Li X, Ross DA, Trusler JPM, Maitland GC, Boek ES. Molecular dynamics simulations of CO_2 and brine interfacial tension at high temperatures and pressures. J Phys Chem B 2013;117(18):5647–52.
[66] Khosharay S, Abolala M, Varaminian F. Modeling the surface tension and surface properties of (CO_2 + H_2O) and (H_2S + H_2O) with gradient theory in combination with sPC – SAFT EOS and a new proposed influence parameter. J Mol Liq 2014;198:292–8.
[67] Chow Y, Maitland GC, Trusler J. Interfacial tensions of the (CO_2 + N_2 + H_2O) system at temperatures of (298 to 448) K and pressures up to 40 MPa. J Chem Thermodyn 2016;93(1):392–403.
[68] Chow YTF. Eriksen K Daniel, Galindo Amparo, Haslam J Andrew, Jackson George, Maitland C Geoffrey, Trusler J P Martin Interfacial tensions of systems comprising water, carbon dioxide and diluent gases at high pressures: Experimental measurements and modelling with SAFT-VR Mie and square-gradient theory. Fluid Phase Equilib 2016;407(1):159–76.
[69] Partovi M, Mosalanezhad M, Lotfi S, Barati-Harooni A, Najafi-Marghmaleki A, Mohammadi AH. On the Estimation of CO_2-Brine Interfacial Tension. J Mol Liq 2017;243:265–72.
[70] Che Ruslan MFA. Modelling CO_2-Brine Interfacial Tension using Density Gradient Theory. *Physical Science and Engineering (PSE) Division.* Earth Science and Engineering. King Abdullah University of Science & Technology; 2018.
[71] Liu X, Mutailipu M, Zhao J, Liu Y. Comparative analysis of four neural network models on the estimation of CO_2–brine interfacial tension. ACS Omega 2021;6(6):4282–8.
[72] Song Y, Sung W, Jang Y, Jung W. Application of an artificial neural network in predicting the effectiveness of trapping mechanisms on CO_2 sequestration in saline aquifers. Int J Control 2020;98:103042.
[73] Jerauld GR, Kazemi A. An improved simple correlation for accurate estimation of CO_2-Brine interfacial tension at reservoir conditions. J Pet Sci Eng 2022;208:109537.
[74] Amooie MA, Hemmati-Sarapardeh A, Karan K, Husein MM, Soltanian MR, Dabir B. Data-driven modeling of interfacial tension in impure CO_2-brine systems with implications for geological carbon storage. Int J Control 2019;90:102811.
[75] Wagner W, Pruß A. The IAPWS formulation 1995 for the thermodynamic properties of ordinary water substance for general and scientific use. J Phys Chem Ref Data 2002;31(2):387–535.
[76] McBride-Wright M, Maitland GC, Trusler JPM. Viscosity and density of aqueous solutions of carbon dioxide at temperatures from (274 to 449) K and at pressures up to 100 MPa. J Chem Eng Data 2015;60(1):171–80.
[77] Sedlbauer J, O'Connell JP, Wood RH. A new equation of state for correlation and prediction of standard molal thermodynamic properties of aqueous species at high temperatures and pressures. ChGeo 2000;163(1–4):43–63.
[78] Panagiotopoulos AZ, Reid R C. New mixing rules for cubic equations of state for highly polar asymmetric mixtures. American Chemical Society 1986;ACS Symposium Series(300): 571–82.
[79] Orbey H, Sandler SI. Cubic Equations of State and Their Mixing Rules. Cambridge University Press; 1998.
[80] Hoballah R. On the Solubility of Acid and Sour Gases in Water and Brines Under Reservoir Conditions. *Chemical Engineering.* PhD. Imperial College London; 2017.
[81] Al Ghafri SZS, Forte E, Galindo A, Maitland GC, Trusler JPM. Experimental and Modeling Study of the Phase Behavior of (Heptane + Carbon Dioxide + Water) Mixtures. J Chem Eng Data 2015;60(12):3670–81.
[82] Anderson GK. Solubility of Carbon Dioxide in Water under Incipient Clathrate Formation Conditions. J Chem Eng Data 2002;47(2):219–22.
[83] Dalmolin I, Skovroinski E, Biasi A, Corazza ML, Dariva C, Oliveira JV. Solubility of carbon dioxide in binary and ternary mixtures with ethanol and water. Fluid Phase Equilib 2006;245(2):193–200.
[84] Dell'Era C, Uusi-Kyyny P, Pokki J-P, Pakkanen M, Alopaeus V. Solubility of carbon dioxide in aqueous solutions of diisopropanolamine and methyldiethanolamine. Fluid Phase Equilib 2010;293(1):101–9.
[85] Ferrentino G, Barletta D, Balaban MO, Ferrari G, Poletto M. Measurement and prediction of CO_2 solubility in sodium phosphate monobasic solutions for food treatment with high pressure carbon dioxide. J Supercrit Fluids 2010;52(1):142–50.
[86] Foltran S, Vosper ME, Suleiman NB, Wriglesworth A, Ke J, Drage TC, et al. Understanding the solubility of water in carbon capture and storage mixtures: An FTIR spectroscopic study of H_2O+CO_2+N_2 ternary mixtures. Int J Control 2015;35:131–7.
[87] Han JM, Shin HY, Min B-M, Han K-H, Cho A. Measurement and correlation of high pressure phase behavior of carbon dioxide+water system. J Ind Eng Chem 2009;15(2):212–6.
[88] Iwai Y, Uno M, Nagano H, Arai Y. Measurement of solubilities of palmitic acid in supercritical carbon dioxide and entrainer effect of water by FTIR spectroscopy. J Supercrit Fluids 2004;28(2):193–200.
[89] Kiepe J, Horstmann S, Fischer K, Gmehling J. Experimental determination and prediction of gas solubility data for CO_2 + H_2O mixtures containing NaCl or KCl at temperatures between 313 and 393 K and pressures up to 10 MPa. Ind Eng Chem Res 2002;41:4393–8.
[90] Krotov DG, Jürgen; Brehm, Axel Further development of the group contribution equation of state VTPR for description of electrolyte and polymer systems. Oldenburg, Univ, Diss 2014.
[91] Liu Y, Hou M, Yang G, Han B. Solubility of CO_2 in aqueous solutions of NaCl, KCl, $CaCl_2$ and their mixed salts at different temperatures and pressures. J Supercrit Fluids 2011;56(2):125–9.

[92] Liu Y, Hou M, Ning H, Yang D, Yang G, Han B. Phase equilibria of $CO_2 + N_2 + H_2O$ and $N_2 + CO_2 + H_2O + NaCl + KCl + CaCl_2$ systems at different temperatures and pressures. J Chem Eng Data 2012;57:1928–32.

[93] Martín Á, Pham HM, Kilzer A, Kareth S, Weidner E. Phase equilibria of carbon dioxide+poly ethylene glycol+water mixtures at high pressure: Measurements and modelling. Fluid Phase Equilib 2009;286(2):162–9.

[94] Meyer CW, Harvey AH. Dew-point measurements for water in compressed carbon dioxide. AIChE 2015;61(9):2913–25.

[95] Muromachi S, Shijima A, Miyamoto H, Ohmura R. Experimental measurements of carbon dioxide solubility in aqueous tetra-n-butylammonium bromide solutions. J Chem Thermodyn 2015;85:94–100.

[96] Qin J, Rosenbauer RJ, Duan Z. Experimental Measurements of Vapor-Liquid Equilibria of the $H_2O + CO_2 + CH_4$ Ternary System. J Chem Eng Data 2008;53 (6):1246–9.

[97] Ruffine L, Trusler JPM. Phase behaviour of mixed-gas hydrate systems containing carbon dioxide. J Chem Thermodyn 2010;42(5):605–11.

[98] Schüler N, Hecht K, Kraut M, Dittmeyer R. On the Solubility of Carbon Dioxide in Binary Water-Methanol Mixtures. J Chem Eng Data 2012;57:2304–8.

[99] Serpa FS, Vidal RS, Filho JHBA, Nascimento JF, Ciambelli JRP, Figueiredo CMS, et al. Solubility of Carbon Dioxide in Ethane-1,2-diol–Water Mixtures. J Chem Eng Data 2013;58(12):3464–9.

[100] Servio P, Englezos P. Effect of temperature and pressure on the solubility of carbon dioxide in water in the presence of gas hydrate. Fluid Phase Equilib 2001; 190(1):127–34.

[101] Tang Y, Bian X, Du Z, Wang C. Measurement and prediction model of carbon dioxide solubility in aqueous solutions containing bicarbonate anion. Fluid Phase Equilib 2015;386:56–64.

[102] Tong D, Trusler M, Vega-Maza D. Solubility of CO_2 in Aqueous Solutions of $CaCl_2$ or $MgCl_2$ and in a Synthetic Formation Brine at Temperatures up to 423 K and Pressures up to 40 MPa. J Chem Eng Data 2013;58:2116–24.

[103] Wang Z, Felmy AR, Thompson CJ, Loring JS, Joly AG, Rosso KM, et al. Near-infrared spectroscopic investigation of water in supercritical CO_2 and the effect of $CaCl_2$. Fluid Phase Equilib 2013;338:155–63.

[104] Zhang G, Wu Y, Ma P, Wu G, Li D. Measurement and correlation of solubility of carbon monoxide and other gases solubility in phenol. Huagong Xuebao/Journal of Chemical Industry and Engineering (China) 2005;56:2039–45.

[105] Koschel D, Coxam J-Y, Rodier L, Majer V. Enthalpy and solubility data of CO_2 in water and NaCl(aq) at conditions of interest for geological sequestration. Fluid Phase Equilib 2006;247(1):107–20.

[106] Nighswander JA, Kalogerakis N, Mehrotra AK. Solubilities of carbon dioxide in water and 1 wt. % sodium chloride solution at pressures up to 10 MPa and temperatures from 80 to 200.degree.C. J Chem Eng Data 1989;34(3):355–60.

[107] Guo H, Huang Y, Chen Y, Zhou Q. Quantitative Raman Spectroscopic Measurements of CO_2 Solubility in NaCl Solution from (273.15 to 473.15) K at p = (10.0, 20.0, 30.0, and 40.0) MPa. J Chem Eng Data 2016;61(1):466-74.

[108] Zhao H, Dilmore R, Allen DE, Hedges SW, Soong Y, Lvov SN. Measurement and modeling of CO_2 solubility in natural and synthetic formation brines for CO_2 sequestration. Environ Sci Tech 2015;49(3):1972–80.

[109] dos Santos PF, André L, Ducousso M, Lassin A, Contamine F, Lach A, et al. An improved model for CO_2 solubility in aqueous Na^+–Cl^-–SO_4^{2-} systems up to 473.15 K and 40 MPa. Chemical Geology 2021;582:120443.

[110] Han X, Yu Z, Qu J, Qi T, Guo W, Zhang G. Measurement and Correlation of Solubility Data for CO_2 in $NaHCO_3$ Aqueous Solution. J Chem Eng Data 2011;56 (4):1213–9.

[111] Georgiadis A, Llovell F, Bismarck A, Blas FJ, Galindo A, Maitland GC, et al. Interfacial tension measurements and modelling of (carbon dioxide+n-alkane) and (carbon dioxide+water) binary mixtures at elevated pressures and temperatures. J Supercrit Fluids 2010;55(2):743–54.

[112] Florence YTC. Maitland C Geoffrey, Trusler J P Martin Interfacial tensions of the ($CO_2 + N_2 + H_2O$) system at temperatures of (298 to 448) K and pressures up to 40 MPa. J Chem Thermodyn 2016;93(1):392–403.

[113] IAPWS. Revised Release on Surface Tension of Ordinary Water Substance - June 2014; 2014. Available from: http://www.iapws.org/relguide/Surf-H2O.html. [Accessed 9 Jan 2023.

[114] Li XS, Boek E, Maitland GC, Trusler JPM. Interfacial Tension of (Brines + CO_2): (0.864 NaCl+0.136 KCl) at Temperatures between (298 and 448) K, Pressures between (2 and 50) MPa, and Total Molalities of (1 to 5) mol/kg. J Chem Eng Data 2012;57(4):1078–88.

[115] Hebach A, Oberhof A, Dahmen N, Kögel A, Ederer H, Dinjus E. Interfacial tension at elevated pressures measurements and correlations in the water+ carbon dioxide system. J Chem Eng Data 2002;47(6):1540–6.

[116] Li XS, Boek ES, Maitland GC, Trusler JPM. Interfacial Tension of (Brines+CO_2): $CaCl_2$(aq), $MgCl_2$(aq), and Na_2SO_4(aq) at Temperatures between (343 and 423) K, Pressures between (2 and 50) MPa, and Molalities of (0.5 to 5) mol.kg^{-1}. J Chem Eng Data 2012;57(5):1369–75.

[117] Pereira LMC, Chapoy A, Burgass R, Oliveira MB, Coutinho JAP, Tohidi B. Study of the impact of high temperatures and pressures on the equilibrium densities and interfacial tension of the carbon dioxide/water system. J Chem Thermodyn 2016; 93:404–15.

[118] Khosharay SV, F.. Experimental and modeling investigation on surface tension and surface properties of ($CH_4 + H_2O$), ($C_2H_6 + H_2O$), ($CO_2 + H_2O$) and ($C_3H_8 + H_2O$) from 284.15 K to 312.15 K and pressures up to 60 bar. Int J Refrig 2014;47: 26–35.

[119] Li X. Interfacial Properties of Reservoir Fluids and Rocks. Chemical Engineering. PhD. London: Imperial College London; 2013.

[120] Chiquet P, Daridon J-L, Broseta D, Thibeau S. CO_2/water interfacial tensions under pressure and temperature conditions of CO_2 geological storage. Energ Conver Manage 2007;48(3):736–44.

[121] Liu Y, Tang J, Wang M, Wang Q, Tong J, Zhao J, et al. Measurement of Interfacial Tension of CO_2 and NaCl Aqueous Solution over Wide Temperature, Pressure, and Salinity Ranges. J Chem Eng Data 2017;62(3):1036–46.

[122] Bachu S, Bennion DB. Interfacial Tension between CO_2, Freshwater, and Brine in the Range of Pressure from (2 to 27) MPa, Temperature from (20 to 125) degrees C, and Water Salinity from (0 to 334 000) mg/L^{-1}. J Chem Eng Data 2009;54(3): 765–75.

[123] Chun B-S, Wilkinson GT. Interfacial tension in high-pressure carbon dioxide mixtures. Ind Eng Chem Res 1995;34(12):4371–7.

[124] Jho C, Nealon D, Shogbola S, King Jr AD. Effect of Pressure on the Surface Tension of Water: Adsorption of Hydrocarbon Gases and Carbon Dioxide on Water at Temperatures between 0 and 50°C. J COLLOID INTERF SCI 1978;65(1): 141–54.

[125] Bikkina PK, Shoham O, Uppaluri R. Equilibrated Interfacial Tension Data of the CO_2–Water System at High Pressures and Moderate Temperatures. J Chem Eng Data 2011;56(10):3725–33.

[126] Liu Y. Li Huazhou Andy, Okuno Ryosuke Measurements and Modeling of Interfacial Tension for CO_2/CH_4/Brine Systems under Reservoir Conditions. Ind Eng Chem Res 2016;55(48):12358–75.

[127] Pereira LMC, Chapoy A, Burgass R, Tohidi B. Interfacial tension of CO_2 + brine systems: Experiments and predictive modelling. Adv Water Resour 2017;103(1): 64–75.

[128] Aggelopoulos CA, Robin M, Perfetti E, Vizika O. $CO_2/CaCl_2$ solution interfacial tensions under CO_2 geological storage conditions: Influence of cation valence on interfacial tension. Adv Water Resour 2010;33(6):691–7.

[129] Aggelopoulos C, Robin M, Vizika O. Interfacial tension between CO_2 and brine (NaCl+ $CaCl_2$) at elevated pressures and temperatures: The additive effect of different salts. Adv Water Resour 2011;34(4):505–11.

[130] Meiheriayi Mutailipu YL, Jiang L, Zhang Yi. Measurement and estimation of CO_2–brine interfacial tension and rock wettability under CO_2 sub- and super-critical conditions. J Colloid Interface Sci 2019;534:605–17.